

A population of main belt asteroids co-orbiting with Ceres and Vesta

Apostolos A. Christou^{a,*}, Paul Wiegert^b

^a*Armagh Observatory, College Hill, Armagh BT61 9DG, Northern Ireland, UK*

^b*The University of Western Ontario, Department of Physics and Astronomy, London, Ontario N6A 3K7, Canada*

Abstract

We have carried out a search for Main Belt Asteroids (MBAs) co-orbiting with the large MBA Vesta and the dwarf planet Ceres. Through improving the search criteria used in Christou (2000b) and numerical integrations of candidate coorbitals, we have identified approximately 51 (44) objects currently in co-orbital libration with Ceres (Vesta). We show that these form part of a larger population of transient coorbitals; 129 (94) MBAs undergo episodes of co-orbital libration with Ceres (Vesta) within a 2 Myr interval centred on the present. The lifetime in the resonance is typically a few times $\sim 10^5$ yr but can exceed 2×10^6 yr. The variational properties of the orbits of several co-orbitals were examined. It was found that their present states with respect to the secondary are well determined but knowledge of it is lost typically after $\sim 2 \times 10^5$ years. Objects initially deeper into the coorbital region maintain their coorbital state for longer. Using the model of Namouni et al. (1999) we show that their dynamics are similar to those of temporary coorbital NEAs of the Earth and Venus. As in that case, the lifetime of resonant libration is dictated by planetary secular perturbations, the inherent chaoticity of the orbits and close encounters with massive objects other than the secondary. In particular we present evidence that, while in the coorbital state, close encounters with the secondary are generally avoided and that Ceres affects the stability of tadpole librators of Vesta. Finally we demonstrate the existence of Quasi-satellite orbiters of both Ceres and Vesta

*Corresponding author

Email addresses: aac@arm.ac.uk (Apostolos A. Christou), **Fax:** +44 2837 522928 (Apostolos A. Christou), pwiegert@uwo.ca (Paul Wiegert)

and conclude that decametre-sized objects detected in the vicinity of Vesta by the DAWN mission may, in fact, belong to this dynamical class rather than be bona-fide (i.e. keplerian) satellites of Vesta.

Keywords: Asteroids, Dynamics, Asteroid Ceres, Asteroid Vesta

1. Introduction

The coorbital resonance, where the gravitational interaction between two bodies with nearly the same orbital energy leads to stable and predictable motion, is ubiquitous in the solar system. Objects attended by known co-orbital companions include Jupiter, Mars as well as the saturnian satellites Tethys, Dione, Janus and Epimetheus (see Christou, 2000a, for a review). More recently, the planet Neptune was added to this list (Sheppard and Trujillo, 2006) while an additional coorbital of Dione was discovered by the *Cassini* mission (Murray et al., 2005). In all these cases, the motion has been shown to be stable against all but the most slow-acting perturbations (Lissauer et al., 1985; Levison et al., 1997; Brasser et al., 2004; Scholl et al., 2005).

The discovery of a coorbital attendant of the Earth on a highly inclined and eccentric orbit (Wiegert et al., 1997, 1998) motivated new theoretical work in the field. Namouni (1999), using Hill’s approximation to the Restricted Three Body Problem (R3BP) showed analytically that the introduction of large eccentricity and inclination modifies considerably the topology of coorbital dynamics near the secondary mass. It results in the appearance of bounded eccentric orbits (Quasi-Satellites; Mikkola and Innanen, 1997) and, in three dimensions, “compound” orbits and stable transitions between the different modes of libration. Further, he demonstrated numerically that these results hold when the full R3BP is considered. In this case, the appearance of new types of compound orbits, such as asymmetric modes or compounds of tadpoles and retrograde satellites, was shown in Namouni et al. (1999) to be due to the secular evolution of the coorbital potential. Such types of coorbital libration were identified in the motion of the object highlighted by Wiegert et al. (1997) as well as other near-Earth asteroids but the secular forcing of the potential in that case is provided by planetary secular perturbations (Namouni et al., 1999; Christou, 2000a). The expected characteristics of the population of co-orbitals of Earth and Venus were investigated by Morais and Morbidelli (2002) and Morais and Morbidelli (2006) respectively.

Christou (2000b), motivated by Pluto’s ability, as demonstrated by Yu and Tremaine

(1999) and Nesvorný et al. (2000), to trap other Edgeworth-Kuiper Belt objects in co-orbital motion with itself, demonstrated in turn that main belt asteroids can co-orbit with the dwarf planet 1 Ceres and the large Main Belt Asteroid (MBA) 4 Vesta. Four such asteroids were identified, two co-orbiting with Ceres and two with Vesta.

Here we report the results of a search for additional coorbitals of these two massive asteroids. This was motivated partly by the large growth in the number of sufficiently well-known MBA orbits during the intervening decade, but also a refinement of the search criterion used in the work by Christou. As a result, we find over 200 new transient co-orbital MBAs of Ceres and Vesta. In this work we examine their ensemble properties, use existing dynamical models to understand how they arise and identify similarities with co-orbital populations elsewhere in the solar system, in particular the transient co-orbital NEAs of Earth and Venus.

The paper is organised as follows: In the next Section we expose our Search methodology, in particular those aspects which differ from the search carried out by Christou (2000b). In Section 3 we describe the statistics of coorbital lifetime and orbital element distribution found in our integrations. In addition, we examine the robustness of the dynamical structures we observe. In Section 4 we investigate the degree to which the model of Namouni et al. (1999) can reproduce the observed dynamics. Section 5 deals with the effects of additional massive asteroids in the three-body dynamics while Section 6 focuses on the stability of so-called Quasi-Satellite orbits. Finally, Section 7 summarises our conclusions and identifies further avenues of investigation.

2. Search Methodology

Christou (2000b) searched for candidate Ceres coorbitals by employing the osculating semimajor axis a_r of the asteroid relative to that of Ceres (equal to $(a - a_{\text{Ceres}})/a_{\text{Ceres}}$) to highlight objects that merited further investigation. This method, although it led to the successful identification of two coorbitals, 1372 Haremaria and 8877 Rentaro, ignores the existence of high frequency variations in a due to perturbations by the planets, especially Jupiter. This is illustrated in the upper panel of Fig. 1 where the evolution of a_r for asteroid 1372 Haremaria, one of the objects identified by Christou, is depicted. A periodic term of amplitude 0.001 apparently causes a_r to move in and out of Ceres' coorbital zone (bounded by the dashed horizontal lines)

68 every 20 years. On the other hand, an object with $a_r \leq \epsilon$ would have a con-
 69 junction with Ceres every $\geq 6 \times 10^4$ years. Here $\epsilon = (\mu/3)^{1/3}$ denotes Hill's
 70 parameter in the Circular Restricted Three-Body Problem for a secondary
 71 body with a mass μ scaled to that of the central body (in this case, the Sun).
 72 This suggests that coorbital motion should be insensitive to these variations
 73 and that a low-pass filtered semimajor axis would work better as an indicator
 74 of libration in the 1:1 resonance with Ceres. We have chosen this to be the
 75 synthetic proper semimajor axis (hereafter referred to as “proper semimajor
 76 axis”) as defined by Knežević and Milani (2000). Synthetic proper elements
 77 are numerically-derived constants of an asteroid's motion under planetary
 78 perturbations. The proper semimajor axis, in particular, is invariant with
 79 respect to secular perturbations up to the second order in the masses under
 80 Poisson's theorem and, hence, an appropriate metric to use in this work. In
 81 the bottom panel of Fig. 1, we plotted the proper relative semimajor axis
 82 $a_{r, p} = (a_p - a_{p, \text{Ceres}}) / a_{p, \text{Ceres}}$; bold horizontal line) superimposed on the
 83 a_r history of the asteroid but filtered with a 256-point running-box average.
 84 The slopes at the beginning and the end of this time series are the result
 85 of incomplete averaging. The dots in the bottom panel represent the un-
 86 averaged osculating semimajor axis sampled with a constant timestep of 1
 87 yr. It is observed that the proper semimajor axis agrees with the average of
 88 its osculating counterpart, whereas the osculating value sampled at $t = 0$ (
 89 Julian Date 2451545.0; dashed horizontal line) does not.

90 For our search we used the database of synthetic proper elements for
 91 185546 numbered asteroids computed by Novaković, Knežević and Milani
 92 that was available as of 09/2008 at the *AstDys* online information service
 93 (<http://hamilton.dm.unipi.it/~astdys/propsynth/numb.syn>). A total of 648
 94 and 514 main-belt asteroids respectively with proper semimajor axes within
 95 $\pm a\epsilon$ of those of Ceres and Vesta were identified. Table 1 shows the pa-
 96 rameters relevant to this search for the massive asteroids. The second row
 97 provides the mass ratio μ of the asteroid relative to the mass of the Sun, the
 98 third row its Hill parameter ϵ , the fourth row the asteroids' synthetic proper
 99 semimajor axis a_p as given in the database and the fifth row the product
 100 $a_p \times \epsilon$ which is the half-width of the coorbital region in AU.

101 The state vectors of these asteroids at Julian Date 2451545.0 were re-
 102 trieved from HORIZONS (Giorgini et al., 1996) and numerically integrated
 103 one million years in the past and in the future using a model of the solar
 104 system consisting of the 8 major planets and the asteroids 1 Ceres, 4 Vesta,
 105 2 Pallas and 10 Hygiea. Mass values adopted for these four asteroids were

106 taken from Konopliv et al. (2006). Their initial state vectors as well as plan-
 107 etary initial conditions and constants were also retrieved from HORIZONS.
 108 The integrations were carried out using the “hybrid” scheme which is part
 109 of the MERCURY package (Chambers, 1999). This scheme is based on a
 110 second-order mixed variable symplectic (MVS) algorithm; it switches to a
 111 Bulirsch-Stoer scheme within a certain distance from a massive object. For
 112 all the integrations reported here, this distance was 5 Hill radii. A time step
 113 of 4 days or $\sim 1/20$ th of the orbital period of Mercury was chosen in order
 114 to mitigate the effects of stepsize resonances (Wisdom and Holman, 1992).
 115 Trials of this scheme vs an RA15 RADAU integrator (Everhart, 1985) in-
 116 cluded in the same package and with a tolerance parameter of 10^{-13} showed
 117 the results to be indistinguishable from each other while the hybrid scheme
 118 was significantly faster.

119 **3. Results**

120 *3.1. Population Statistics*

121 In our runs, we observed a total of 129 and 94 asteroids enter in one of
 122 the known libration modes of the 1:1 resonance with Ceres or Vesta respec-
 123 tively at some point during the integrations. A full list of these asteroids
 124 is available from the corresponding author upon request. Table 2 shows a
 125 statistical breakdown of the observed population according to different types
 126 of behaviour. The first row identifies the secondary (Ceres or Vesta). The
 127 top part of the Table shows the number of asteroids that were captured into
 128 co-orbital libration at some point during the 2×10^6 yr simulation (second
 129 column), the number of asteroids that were found to be co-orbiting at present
 130 (“current” coorbitals; third column) and the number of current L_4 and L_5
 131 tadpole librators (fourth and fifth rows respectively). The bottom part of
 132 the table shows the number of current horseshoe librators (second column),
 133 the number of objects currently in transition between two distinct libration
 134 modes (third column) and the number of current Quasi-Satellite (QS) libra-
 135 tors. The fifth column shows the number of asteroids that were librating
 136 for the full duration of the numerical integration, although not necessarily
 137 in the same mode (“persistent” coorbitals). Numbers in brackets refer to
 138 MBAs that remained in the same libration mode throughout the integration
 139 (“single mode persistent” coorbitals). A total of 95 MBAs are currently in
 140 the 1:1 resonance with either Ceres or Vesta with the ratio of objects cor-
 141 responding to the two asteroids (51/44) being roughly the same as for the

original sample (129/94). The number of MBAs currently in tadpole orbits is 19 and 12 for the two asteroids respectively while horseshoes are evenly matched at 20 and 21. 11 objects for each asteroid are in the process of transitioning between different modes of libration. One object, MBA 76146, is currently in a Quasi-Satellite (QS) orbit around Ceres with a guiding centre amplitude of $\sim 10^\circ$ in λ_r (rightmost panels in Fig 2) while two other MBAs, 138245 and 166529, are currently transitioning into such a state.

3.2. Some Examples

In most cases, the librations were transient i.e. changing to another mode or to circulation of the critical argument $\lambda_r = \lambda - \lambda_{\text{Ceres/Vesta}}$. In that sense, there is a similarity to what is observed for co-orbitals of the Earth and Venus (Namouni et al., 1999; Christou, 2000a; Morais and Morbidelli, 2002, 2006). Compound modes (unions of Quasi-Satellite and Horseshoe or Tadpole librations) also appear, although they are rare. Examples of different types of behaviour are shown in Figs 2 and 3 for Ceres and Vesta respectively.

In the former case, asteroid 71210 (left column) is currently ($t = 0$ at Julian Date 2451545.0) in a horseshoe configuration with Ceres, transitioning to tadpole libration at times. The position of Ceres at $\lambda_r = 0$ is avoided. Asteroid 81522 (centre column) librates around the L_4 triangular equilibrium point of Ceres for the duration of the integration. In the right column we observe stable transitions of the orbit of asteroid 76146 between different libration modes. The maximum excursion of the guiding centre of the asteroid from that of Ceres during the integration is $a_r = 10^{-4}$ or 0.2ϵ , well within the coorbital region. This asteroid becomes a Quasi-Satellite of Ceres at $t = -2 \times 10^5$ yr and transitions into a horseshoe mode at $t = +10^5$ yr.

In the case of Vesta, asteroid 22668 (left column) transitions from a passing to a horseshoe mode and back again. It is currently a horseshoe of Vesta. Near the end of the integration it enters into Quasi-Satellite libration with Vesta, where it remains. At $t = +5 \times 10^5$ yr it executes half a libration in a compound Horseshoe/Quasi Satellite mode. Asteroid 98231 (centre column) is an L_5 tadpole of Vesta at $t = -1 \times 10^6$ yr. The libration amplitude increases gradually until transition into horseshoe libration occurs at $t = -3 \times 10^5$ yr. During this period the libration amplitude begins to decrease until the reverse transition back into L_4 libration takes place at $t = +6 \times 10^5$ yr. This behaviour should be compared with the case of asteroid 71210 in Fig. 2. The evolution of asteroid 156810 (right column) is similar to that of 98231 except

178 that the rate of increase of the libration amplitude reverses sign before tran-
 179 sition into horseshoe libration takes place. As a result, the asteroid librates
 180 around the L_4 equilibrium point of Vesta for the duration of the integration.

181 3.3. Variational Properties

182 Although these results can be regarded statistically, their value is in-
 183 creased if we establish their robustness against the ephemeris uncertainties
 184 of the asteroids. To investigate this, we have picked 6 asteroids in the sam-
 185 ple, populated their 1-sigma uncertainty ellipsoids with 100 clones per object
 186 using states and state covariance matrices retrieved from the *AstDys* online
 187 orbital information service, and propagated them forward in time for 10^6 yr
 188 under the same model of the solar system as before but using an integrator
 189 developed by one of us (PW) with a 4-day time step. This code utilises the
 190 same algorithm as the HYBRID code within MERCURY. In the original inte-
 191 grations, 65313 and 129109 persist as L_5 Trojans of Ceres, 81522 and 185105
 192 as L_4 Trojans of Ceres and 156810 persists as an L_5 Trojan of Vesta. Asteroid
 193 76146 is a Quasi-Satellite of Ceres until $+10^5$ yr. Their Lyapounov times,
 194 as given by the proper element database of Novaković et al, are: 3×10^6 ,
 195 5×10^5 , 2×10^6 , 6×10^5 , 10^5 and 5×10^5 yr respectively.

196 The results of this exercise are shown in Fig. 4. We find that all clones of
 197 65313 and 81522 remain as Trojans of Ceres for the full integration. 76146
 198 persists as a Quasi-Satellite of Ceres until $\sim +6 \times 10^5$ yr. Three clones of
 199 129109 escape from libration around L_5 after $\sim 5 \times 10^5$ yr, but most remain
 200 in libration until the end. Those of 185105 begin to diverge at $\sim +3 \times 10^5$
 201 yr until knowledge of the object's state is lost near the middle of the in-
 202 tegration timespan. The clones of the Vesta Trojan 156810 suffer a simi-
 203 lar fate, but divergence is more general in nature; most of the clones enter
 204 into other libration modes by $+6 \times 10^5$ yr. We conclude that the present
 205 state of these objects, as determined by the original integrations, is robust.
 206 The differences we observe in their evolution could be due to several causes.
 207 Firstly, although we use the same force model and the same type of inte-
 208 grator, the initial states of the asteroids in the new integrations were taken
 209 from AstDys, not HORIZONS, and correspond to a later epoch of oscula-
 210 tion. In addition, the volumes of space sampled by the object's ephemeris
 211 uncertainties, being proportional to the eigenvalue product of the respective
 212 covariance matrices, are smallest for 65313 and 81522. We therefore expect
 213 that, assuming similar Lyapounov times, clones of low-numbered asteroids -
 214 generally those with longer observational arcs - would be slower to disperse

215 than those of high-numbered ones. Interestingly, the clones disperse faster
 216 than one would expect from their Lyapounov times, however some differences
 217 would be expected since the model used to compute these did not include the
 218 gravitational attraction of large asteroids. In Section 5, the role of impulsive
 219 perturbations during close encounters is investigated in detail.

220 3.4. Proper element distribution

221 In order to understand the ensemble properties of the population and
 222 how these might differ from those of other MBAs, we have compared the dis-
 223 tribution of their proper elements to that of the broader population. Fig 5
 224 shows the distribution of the relative proper semimajor axis (blue curve)
 225 $a_{r,p} = (a_p - a_{p, \text{Ceres/Vesta}}) / a_{p, \text{Ceres/Vesta}}$ of these MBAs, scaled to ϵ , super-
 226 posed on that of all MBAs in the interval $[-2\epsilon, +2\epsilon]$ (red curve). The width
 227 of each bin for both panels is 0.06. The sharp peak at $a_r = -1.2$ in the
 228 plot for Vesta reflects an increased concentration of asteroid proper elements
 229 probably associated with the 36:11 mean motion resonance with Jupiter. Al-
 230 though interesting in its own right, we do not, at present, have reason to
 231 believe that its existence near the co-orbital region of Vesta is anything more
 232 than coincidental. Hence, we refrain from discussing it further in this paper.

233 In both cases, the distributions appear to be centred at $a_{r,p} = 0$. Gaus-
 234 sian fits to the centre μ and the standard deviation σ of the distribution give
 235 a Full Width at Half Maximum (FWHM; $2\sqrt{2\log 2}\sigma$) of 0.334 ± 0.033 and a
 236 centre at -0.053 ± 0.017 for the Ceres distribution. The slight offset to the
 237 left is probably due to slightly higher counts for the bins left of $a_{r,p} = 0$.
 238 The Vesta distribution is slightly narrower (FWHM of 0.292 ± 0.028) but
 239 more symmetric around the origin (centre at -0.006 ± 0.014). No cases of
 240 coorbital libration were observed for asteroids with $|a_{r,p}| > 0.42$ while only
 241 two cases (both with Vesta) had $|a_{r,p}| > 0.30$.

242 Seeking additional insight into the dependence of the coorbital state on
 243 the semimajor axis, we examined the distributions of different types of co-
 244 orbital - as observed in our simulations - normalised to the total number
 245 of MBAs in each bin. In Fig. 6 we show the distributions of all coorbitals
 246 (red curve), current coorbitals (blue curve) and persistent coorbitals (gray
 247 curve). Fitted values of the Gaussian parameters (μ , FWHM) for the three
 248 populations are given in Table 3. The distributions for Vesta coorbitals
 249 are consistently narrower than those of Ceres implying that this is a real
 250 difference between the two.

Interestingly, both cases exhibit a hierarchy in the three populations: the persistent population is embedded into the current one, which in turn is embedded into the distribution of all objects. One important consequence of this observation is that one can robustly define the boundaries of each population. This is, of course, partly due to the criteria used to define each population but the fact that there are clear differences between the three populations (ie no two populations coincide) is not a trivial one. Hence, persistent coorbitals are confined in the domain $|a_{r,p}| < 0.12$, current coorbitals within $|a_{r,p}| < 0.24$ and all coorbitals in the domain $|a_{r,p}| < 0.42$. The shape of the distributions in Figs. 5 and 6 can be partly attributed to the coorbital dynamics (see Section 4). However, they must also be affected by chaotic ‘noise’ in the determination of the proper elements which we used in our search (Milani and Knežević, 1994). In their 2 Myr integrations, Knežević and Milani (2000) regarded the derived proper elements of MBAs with $\sigma_{a_p} < 3 \times 10^{-4}$, $\sigma_{e_p} < 3 \times 10^{-3}$ and $\sigma_{I_p} < 10^{-3}$ as ‘good’. All but four of the asteroids considered here belong to this category. The bound for the proper semimajor axis corresponds to 20% of the width of the coorbital region of Ceres and 35% of that of Vesta (Table 1). It is also comparable to the fitted widths of the distributions of the coorbitals found here. Hence, the actual distributions are likely significantly altered by a convolution with an error function. On the other hand, this convolution does not completely smear out the true distribution of $a_{r,p}$ since, in that case, the observed sorting of the populations according to residence time in the resonance would not occur (Fig. 6).

The distribution of the proper eccentricities and inclinations of individual coorbitals in relation to those of other MBAs are shown in Fig. 7. Plus symbols denote MBAs that have tested negative for co-orbital motion within the period $[-10^6 \text{ yr}, 10^6 \text{ yr}]$. Asterisks and squares refer to the respective populations of current and persistent coorbitals while the filled circle marks the location of the secondary (either Ceres or Vesta). In the interests of clarity, we have not plotted the distribution of all coorbitals. Instead, we show as triangles those persistent coorbitals that remained in either L_4 or L_5 tadpole libration for the full simulation. Their location deep into the coorbital region are in agreement with the theoretical upper limit - $\sqrt{(8/3)\mu_{\text{Ceres/Vesta}}}$ - for near-planar, near-circular tadpole orbits which evaluates to 0.065ϵ for Ceres and 0.053ϵ for Vesta.

The significant size of the sample of coorbitals under study prompted a search for trends in the distribution of λ_r . Fig. 8 shows a histogram of this

289 quantity at $t = 0$ for all current coorbitals and with a bin size of 30° . On this
 290 we superimpose, as a dashed line, a histogram of all objects which are not
 291 currently coorbiting with either Ceres or Vesta. The vertical line segments
 292 indicate square-root Poissonian uncertainties. There appear to be no features
 293 that stand out above the uncertainties. Hence the coorbital resonance does
 294 not measurably affect the phasing of the populations of current coorbitals
 295 with respect to their secondary in this case.

296 4. Analysis of the Dynamics

297 The dynamical context presents some similarities with coorbitals of the
 298 Earth and Venus such as non-negligible eccentricities and inclinations. Here
 299 we attempt to model the evolution using the framework of the restricted
 300 three body problem where a particle’s state evolves under the gravity of the
 301 Sun and the secondary mass (Namouni et al., 1999). This is done through
 302 the expression

$$a_r^2 = C - \frac{8\mu}{3} S(\lambda_r, e, I, \omega) \quad (1)$$

303 where

$$S = \frac{1}{2\pi} \int_{-\pi}^{\pi} \left(\frac{a_S}{|\mathbf{r} - \mathbf{r}_S|} - \frac{\mathbf{r} \cdot \mathbf{r}_S}{a a_S} \right) d\lambda. \quad (2)$$

304 Here, a , e , I , ω and λ denote the semimajor axis, eccentricity, inclination,
 305 argument of pericentre and mean longitude of the particle’s orbit. The sub-
 306 script “S” is used to denote the same quantities for the secondary. The
 307 heliocentric position vectors of the particle and the secondary are denoted as
 308 \mathbf{r} and \mathbf{r}_S respectively. The relative elements a_r and λ_r are defined as

$$a_r = (a - a_S) / a_S, \lambda_r = \lambda - \lambda_S \quad (3)$$

309 and μ is the mass of the secondary scaled to the total system mass. Eq. 1
 310 can be seen as a conservation law where C is the constant “energy” of the
 311 particle, a_r^2 its kinetic energy and the term containing S its potential energy.
 312 Namouni et al. showed that, as the left-hand side of this expression cannot
 313 be negative, it restricts, in general, the evolution of (a_r, λ_r) . A collision
 314 ($\mathbf{r} = \mathbf{r}_S$) can only occur for specific combinations of values for e , I and ω .
 315 Hence, actual collisions are rare and the above formulation is generally valid.

316 For computational purposes, Eq. 2 may be evaluated using standard two-
 317 body formulae (eg Murray and Dermott, 1999) as $\dot{\lambda} \gg \dot{e}$, \dot{I} , $\dot{\omega}$ and $\dot{\lambda}_r$. One

318 other consideration that is specific to this paper is that the high frequency
 319 harmonics of a are external to the R3BP (hence external to the model) and
 320 must somehow be removed before the above expressions may be used. How-
 321 ever, at $t = 0$, the relative proper semimajor axis $a_{r, p}$ can be considered to
 322 be this low-pass filtered value of a_r in the Sun - Ceres/Vesta - MBA problem
 323 (see also Section 2). Hence, the constant C can be evaluated and the model
 324 can be readily applied. In Fig. 9 we show S profiles for each of the MBAs in
 325 Figs 2 and 3 compared to the location of the point $(\lambda_r, \mathcal{E} = 3C/(8\mu))$ at $t = 0$
 326 (dotted circle). As motion is restricted to the domain above S , the model
 327 predicts that the Ceres coorbitals 71210, 81522, 76146 are currently in L₅
 328 tadpole, L₄ tadpole and Quasi-Satellite libration respectively. Similarly the
 329 Vesta coorbitals 22668, 98231 and 156810 are predicted to be in horseshoe,
 330 horseshoe and L₅ libration respectively. Referring to the Figure, the model
 331 apparently succeeds in 5 out of the 6 cases, but fails in the case of the Ceres
 332 coorbital 71210 where the observed mode of libration is a horseshoe.

333 This is probably due to the fact that Eq 1 is evaluated when $a_r = 0$ i.e.
 334 at the turning points of the libration. In Namouni et al. (1999), $\dot{\lambda}_r \gg \dot{e}$, \dot{I} , $\dot{\omega}$
 335 and the orbit can be considered “frozen” during a libration cycle. In our case,
 336 however, we observe that $\dot{\omega} > \dot{\lambda}_r$ because of the small mass of the secondary.
 337 Incidentally, this parity in timescales may also account for the general lack
 338 of compound libration modes for these coorbitals, as ω controls the relative
 339 height of the maxima of S on either side of $\lambda_r = 0$.

340 To quantify the effect that this has to our model, we evaluated \mathcal{E} against
 341 S for the example MBAs shown in Figs 2 and 3 but at different values of λ_r
 342 and ω . We found that determination of S is generally insensitive to ω , except
 343 near the local maxima bracketing the origin on the λ_r axis. Physically, these
 344 correspond to the closest possible cartesian distances between the particle
 345 and the secondary so it is not a surprise that they are sensitive to the orbital
 346 elements. Particularly for the case where the model failed, $\mathcal{E} - S \simeq 0.6$ when
 347 the asteroid reaches the far end of the model tadpole ($\lambda_r \sim -130^\circ$) and the
 348 potential maximum at $\lambda_r = 180^\circ$ i.e. the object is classified as a horseshoe in
 349 agreement with the numerical integrations. Hence, this method for determin-
 350 ing the resonant mode is formally valid where the object is currently near the
 351 turning point of the libration i.e. those of MBAs 81522, 76146 and 156810.
 352 In the other cases, the more involving process of monitoring the quantity
 353 $\mathcal{E} - S$ in the integrations for a time period comparable to a libration cycle
 354 would be necessary to establish the libration mode.

355 Finally, we wish to understand the stability of the QS librator of Ceres,

76146, in the context of our findings. The sensitivity of S to ω for the local maxima near $\lambda_r = 0$ is important as these features of the potential are the “gatekeepers” for evolution in and out of the QS. This object was captured as a QS from a passing orbit and completes 7 cycles in this mode before becoming a horseshoe. It is currently at $\lambda_r \simeq 8^\circ$. Irrespective of the value of \mathcal{E} , escape from the QS is certain when $S_{t=0} \leq S_{\lambda_r=0}$ i.e. when the extremum at the origin becomes a local maximum. According to the model this occurs for $-34^\circ < \omega < +12^\circ$. Keeping in mind the π periodicity of S in ω , the asteroid will turn back $360/2/46 \sim 4$ times before it escapes, in good agreement with what is observed in the numerical simulation.

5. The role of other massive asteroids

Christou (2000a) showed that Venus and Mars play a key role in the evolution of Earth co-orbitals. These can force transitions between different libration modes or escape from the resonance altogether. Here the only candidates available to play a similar role are other massive asteroids. In this paper we have focused on the effects of Ceres and Vesta - as well as Pallas - on Vesta or Ceres co-orbitals respectively. In a first experiment to determine their role (if any), we have integrated the same six asteroids as in Section 3 but, in the first instance leaving Pallas out of the model (“No Pallas” or NP) and, in the second, only under the gravity of the secondary (ie Ceres or Vesta as appropriate; “Secondary Only” or SO). We find that the evolution of the Ceres Trojans 65313 and 81522 and of the Quasi-Satellite 76146 are the same in both of these runs as well as the original runs where all three massive asteroids were present (“All Masses” or AM). In contrast, we find significant differences in the evolution of the remaining three asteroids, 129109, 156810 and 185105 (Fig. 10). In the SO runs (top row), all clones of these Trojan librators persist as such. This is not the case for the NP and AM runs (middle and bottom rows respectively). Most clones ultimately leave this libration mode, with the exception of 129109 in the AM runs. Although it is difficult, on the basis of a sample of six, to attempt to decouple the effects of the individual massive asteroids, these results indicate that their presence does have an effect on the lifetime of the co-orbital configurations we have found.

To quantify these in a more statistically robust sense, we used MERCURY as before to re-integrate the original 129 and 94 co-orbital MBAs of Ceres and Vesta respectively under the SO, NP and AM models for 10^6 yr in the

392 future (ie half the timespan of the original integrations). We then check which
 393 MBAs survive, either as “persistent” or “single mode” libration in the new
 394 runs. The results are shown in Table 4. As far as persistency is concerned,
 395 the fraction of those co-orbitals in the respective samples is between 20% and
 396 25% for the three models examined (SO, NP and AM) but also for both Ceres
 397 and Vesta co-orbitals. Upon closer inspection, we find that approximately
 398 the same number of persistent co-orbitals (16 for Ceres and 14 for Vesta)
 399 are common between the three models. Thus, Vesta harbours a slightly
 400 larger fraction of these co-orbitals than does Ceres. The remainder of the
 401 persistent population is composed of objects that gain or lose the persistency
 402 property from one model to the next. There is no apparent trend towards one
 403 direction or the other; objects that lose this property are replenished by the
 404 objects which gain it. Thus, it seems that persistency of co-orbital motion is
 405 independent of the adding or removing massive asteroids from the model. If
 406 this premise is correct, then a mechanism that can explain the observations
 407 is the intrinsic chaoticity of the orbits. We saw in Section 3 that the amount
 408 of chaotic ‘noise’ in the proper semimajor axis is comparable to the width of
 409 the coorbital zones of Ceres and Vesta. It is thus reasonable to expect that
 410 some objects are removed from the resonance while others are injected into
 411 it as a consequence of that element’s random walk.

412 The behaviour of single-mode coorbital libration is altogether different.
 413 For Ceres, we find that the addition of other massive asteroids increases the
 414 number of persistent single-mode librators, from 6 (SO) to 14 (NP, AM). For
 415 Vesta, we observe the opposite trend: adding Pallas and Ceres to the model
 416 decreases the number of such librators from 11 (SO) to 3 (NP) and 5 (AM).
 417 In addition, only one object, 87955, persisted as a Ceres L_4 Trojan in all
 418 three models. The statistics are marginally significant for these low counts.
 419 Nevertheless, they compelled us to explore possible causes.

420 It is tempting at this point to try and correlate persistency with the
 421 objects’ Lyapounov Characteristic Exponent (LCE), an established quantifier
 422 of chaoticity, available from the proper element database used in this paper.
 423 However, we point out that these LCEs were computed under a dynamical
 424 model that does not involve any massive asteroids. As it is not clear how
 425 the presence of the co-orbital resonance will affect the determination of the
 426 LCE, we refrain from attempting such a correlation in this work.

427 In Fig. 11 and 12 we present the distribution of the number of Ceres
 428 or Vesta coorbitals respectively that undergo a given number of encounters
 429 within 5 Hill radii ($R_H = a\epsilon$) of the massive asteroids in the three models.

430 A number of interesting features are evident. Firstly, persistent coorbitals
 431 (green and blue columns), as well as a certain fraction of non-persistent coor-
 432 bitals (red columns; 25-30% for Ceres coorbitals, $\sim 50\%$ of Vesta coorbitals),
 433 do not, in general, approach the secondary. This feature was also identified
 434 in Christou (2000a) for Earth co-orbitals (cf Fig. 8 of that paper). It seems to
 435 be a generic feature of coorbital dynamics at high eccentricity and inclination
 436 orbits although the cause-and-effect relationship is not yet clear.

437 In addition, the distribution of encounters for non-persistent coorbitals
 438 (red) shows a tail; in other words, many of these objects undergo many en-
 439 counters with the secondary. This is probably due to the slowness of the evo-
 440 lution of the relative longitude of the guiding centre compared to the epicyclic
 441 motion. Indeed, we find that these encounters are not randomly distributed
 442 in time but occur in groups typically spanning a few centuries. In contrast,
 443 those related to massive asteroids other than the secondary have an upper
 444 cutoff (5 encounters for Pallas and Vesta, 10 for Ceres). The shapes of the
 445 distributions for the three classes of coorbitals are similar. The apparently
 446 high frequencies observed in the case of Ceres encounters for single-mode
 447 persistent coorbitals of Vesta are probably due to the small size of the pop-
 448 ulation in those classes. The better populated distributions in the AM and
 449 SO models mimic the distributions of the other two classes we investigated.

450 A different way to look at the data is to create histograms of minimum
 451 distances, since distance is one of the factors (velocity being the other) that
 452 determine the magnitude of the change in an MBA's orbit. Fig. 13 and
 453 14 show the distribution of these distances in units of R_H . Bin i contains
 454 all recorded encounter distances between $(i - 1) R_H$ and $i R_H$ and have been
 455 normalised with respect to the area of the corresponding annulus of width R_H
 456 on the impact plane. For Ceres coorbitals we do not discern any statistically
 457 significant variations, in other words the counts within the different bins are
 458 the same given the uncertainties. For Vesta coorbitals, the situation is similar
 459 with one exception: we note that single mode persistent coorbitals (blue) do
 460 not approach Ceres closer than one Hill radius. Due to the low counts, we
 461 cannot exclude the possibility that we are looking at statistical variation
 462 in the data. However, if it is the signature of a real trend, it would mean
 463 that encounters with Ceres may cause Vesta coorbitals to exit a particular
 464 libration mode.

465 Regardless of their significance at population level, there is clear evidence
 466 in the data that Ceres encounters can affect the orbital evolution of coorbitals
 467 of Vesta. Fig 15 shows two instances where Vesta coorbital MBAs 45364 and

468 164791 leave the resonance following close encounters with Ceres deep within
 469 the Hill sphere of that dwarf planet. We have searched for similar occurrences
 470 in the evolution of Ceres coorbitals but without success. Neither Pallas nor
 471 Vesta appear capable of playing a similar role. This is probably due to their
 472 smaller masses (hence physically smaller Hill spheres) but also, specifically
 473 for the case of Pallas, the higher encounter velocities.

474 6. Quasi-Satellites

475 This Section is devoted to the existence, as well as stability, of so-called
 476 “Quasi-Satellite” (QS) or “bound” orbits. These appeared first in the lit-
 477 erature as Retrograde Satellite (RS) orbits (as it turned out, a special case
 478 of the QS state; Jackson, 1913) and later studied in the context of dynami-
 479 cal systems analysis (Hénon, 1969; Hénon and Guyot, 1970). More recently,
 480 the survival of this libration mode in the real solar system was examined
 481 by Mikkola and Innanen (1997) and Wiegert et al. (2000). Currently, two
 482 known Quasi-Satellites exist for the Earth (Wajer, 2010) and one for Venus
 483 (Mikkola et al., 2004).

484 Several instances of QS libration relative to Ceres and Vesta were found
 485 in our simulations. Before these are discussed in detail, we introduce some
 486 elements of a convenient theoretical framework to study QS motion dynamics,
 487 namely that by Namouni (1999, see also Henón and Petit, 1986). It employs
 488 the set of relative variables

$$x_r = e_r \cos(nt - \varpi_r) + a_r \quad (4)$$

$$y_r = -2e_r \sin(nt - \varpi_r) + \lambda_r \quad (5)$$

$$z_r = I_r \sin(nt - \Omega_r) \quad (6)$$

489 where n is the mean motion and e_r , I_r , ϖ_r and Ω_r the relative eccentricity,
 490 relative inclination, relative longitude of pericentre and relative longitude of
 491 the ascending node as defined in Namouni (1999) respectively. In this for-
 492 mulation, the motion is composed of the slow evolution of the guiding centre
 493 (a_r, λ_r) to which a fast, three-dimensional epicyclic motion of frequency n
 494 and amplitude proportional to e_r and I_r is superposed. Examples of guiding
 495 centre libration while in QS mode have been shown in Figures 2 (bottom right
 496 panel) and 3 (bottom middle panel). To illustrate the relationship between
 497 the two components of the motion, we show in Fig 16 two examples of QS
 498 motion recovered from our simulations. The left panel shows the cartesian

499 motion of MBA 50251 in a cartesian heliocentric frame that rotates with the
 500 mean motion of Ceres ('C') and for a period of $\sim 5 \times 10^4$ yr. The guiding
 501 centre libration is indicated by the short arc straddling the secondary (actu-
 502 ally a closed loop of width $\sim 10^{-3}$ in a_r) while the cartesian motion along
 503 the epicycle path appears as a loop. The inset shows the evolution of the
 504 relative longitude λ_r for 10^6 yr including the period of libration around 0° .
 505 The example on the right panel shows the motion of MBA 121118 in a frame
 506 rotating with the mean motion of Vesta ('V') during a period of QS libration
 507 around Vesta lasting for 7×10^5 yr. As in the previous case, the guiding cen-
 508 tre libration is indicated by the short arc straddling the secondary. Here, the
 509 higher amplitude of the fast harmonics in the evolution of a_r act to smear
 510 out the epicycle to some extent. It is also evident in these plots that QS
 511 librators are physically located well outside the secondary's Hill sphere and
 512 should not be confused with keplerian satellites.

513 Statistically, we find that 39 (24) out of the 129 (94) Ceres (Vesta) co-
 514 orbitals exhibited QS motion at some point during the 2×10^6 yr period
 515 covered by the simulations reported in Section 3, a fraction of 25-30% in
 516 both cases. In the case of Vesta we find three episodes of QS libration of
 517 unusually long ($> 4 \times 10^5$ yr) duration. One is that of 121118 illustrated in
 518 Fig. 16, the others concern MBAs 22668 and 134633. In Fig. 17 we compare
 519 the distribution of the relative proper semimajor axes of all objects that be-
 520 came temporary QS librators with the members of the persistent coorbital
 521 population. The two are generally separate with the former population fur-
 522 ther away and on either side of the latter. We believe this is because MBAs
 523 capable of becoming Qs are highly energetic. In other words, and referring
 524 to the top left and top right panels of Fig. 9, the value of the energy inte-
 525 gral $3C/8\mu$ - represented by the horizontal line - is generally well separated
 526 from the potential S . Hence the amplitude of a_r libration is only small near
 527 $\lambda_r = 0^\circ$ i.e. if the object is in QS mode at $t = 0$. This is the case for the
 528 one current and the two imminent QS orbiters of Ceres: 76146, 138245 and
 529 166529. The values of a_r for these objects are -0.0068 , -0.0155 and -0.0083
 530 respectively.

531 A particularly interesting subtype of QS liblator is that with vanishing
 532 guiding centre amplitude. These are the "retrograde satellites" (RS orbits)
 533 of Jackson (1913). In that case, the motion can be studied through an energy
 534 integral analogous to Eq. 1 but valid only in Hill's approximation to motion
 535 near the secondary. It depends explicitly on e_r , I_r , ω_r and Ω_r (cf Eqs. 28 and
 536 29 of N99).

537 Activating the QS mode requires $e_r \gg \epsilon$ while physical proximity of the
 538 object to the secondary in an RS orbit is controlled by e_r , I_r and ω_r . For
 539 the small values of ϵ considered here, the relative eccentricity can still be
 540 small in absolute terms (eg 10ϵ or $\sim 10^{-2}$). If I_r is also small (typically
 541 $< e_r$ for bound orbits; see Namouni, 1999), then such objects can remain,
 542 in principle, within a few times 10^6 km of Ceres or Vesta. Note that small
 543 e_r implies a small libration amplitude for λ_r since $\lambda_r < e_r$ (see Section 3.3
 544 of N99). The long-term stability of these configurations depends, through
 545 the energy integral, on the evolution of the relative orbital elements. If these
 546 vary slowly, the asteroid remains trapped in QS motion for many libration
 547 cycles.

548 To model the secular evolution of the asteroid's orbit we need a theoret-
 549 ical model of co-orbital motion within an N-body system. Such models do
 550 exist (eg the theory of Message, 1966 valid near L4 and L5 and the more gen-
 551 eral model of Morais, 1999, 2001). However, the case in hand violates several
 552 assumptions for which those theories are strictly valid: low to moderate e
 553 and I of the asteroid (here $e, I \gg \epsilon$), a coorbital mode (QS) that was not ex-
 554 amined in those works and a clear separation of timescales between coorbital
 555 motion and the secular evolution of the orbit with $\dot{\varpi}, \dot{\Omega} \ll \dot{\lambda}$ (in fact, here we
 556 observe that $\dot{\lambda} < \dot{\varpi}, \dot{\Omega}$). To check that the secular evolution of e , I , ϖ and Ω
 557 of the asteroids does not depend on the presence or absence of the secondary
 558 mass we integrated the orbit of Vesta coorbital MBA 139168 with the eight
 559 major planets both with and without the massive asteroids (including Vesta)
 560 for 1 Myr. We found that the differences in the eccentricity and inclination
 561 vectors - $e \exp i\varpi$ and $I \exp i\Omega$ respectively - are $< 5\%$ between the two cases.
 562 In addition, the asteroids' elements do not exhibit any of the features that
 563 arise from the three-body dynamics (Namouni, 1999). Hence, it is reasonable
 564 to assume that the secular forcing of e_r and I_r is fully decoupled from the
 565 coorbital dynamics and can be modelled by N-body secular theory.

566 In the absence of mean motion resonances, the secular evolution of the
 567 eccentricity and inclination vectors within a system of N bodies in near-
 568 circular, near-planar orbits around a central mass can be approximated by
 569 the so-called Laplace-Lagrange system of $2N$ first order coupled differential
 570 equations which are linear in e and I (Murray & Dermott 1999). The cor-
 571 responding secular solution for the eccentricity and inclination vectors of a
 572 particle introduced into that system has the form of a sum of $N+1$ -periodic

573 complex functions:

$$\mathbf{e} = e_f \exp i(g_f t + \beta_f) + \sum_{i=1}^N E_i \exp i(g_i t + \beta_i) \quad (7)$$

$$\mathbf{I} = I_f \exp i(s_f t + \gamma_f) + \sum_{i=1}^N I_i \exp i(s_i t + \gamma_i) \quad (8)$$

574 where the first and second terms on the right-hand-side are referred to as
 575 the *free* and *forced* components respectively. The parameters of the forced
 576 component are derived directly from the Laplace-Lagrange solution. They,
 577 as well as the free eigenfrequencies g_f and s_f , are dependent only on the
 578 semimajor axes of the planets and the particle.

579 As with the theory of Morais, the validity of these expressions is limited to
 580 low-to-moderate e , I and $g_f \neq g_i$, $s_f \neq s_i$. Brouwer & van Woerkom (1950)
 581 showed that the 5:2 near-resonance between Jupiter and Saturn modifies
 582 the Laplace-Lagrange parameters of the real solar system. However, the
 583 independence of the forced component on the particle's e and I still holds;
 584 this allows us to write

$$\mathbf{e}_r = e_f \exp i(g_f t + \beta_f) - e_f^* \exp i(g_f^* t + \beta_f^*) \quad (9)$$

$$\mathbf{I}_r = I_f \exp i(s_f t + \gamma_f) - I_f^* \exp i(s_f^* t + \gamma_f^*) \quad (10)$$

585 where the superscript ‘ \star ’ refers to Ceres or Vesta as appropriate. Hence, e_r
 586 and I_r are given by

$$e_r = e_f^2 + e_f^{*2} + 2e_f e_f^* \cos [(g_f - g_f^*) t + (\beta_f - \beta_f^*)] \quad (11)$$

$$I_r = I_f^2 + I_f^{*2} + 2I_f I_f^* \cos [(s_f - s_f^*) t + (\gamma_f - \gamma_f^*)] \quad (12)$$

587 The requirement for slow-evolving e_r and I_r implies $g_f \simeq g_f^*$, $s_f \simeq s_f^*$. Fur-
 588 ther, a necessary but not sufficient condition for e_r and I_r to be small is
 589 $e_f \simeq e_f^*$, $I_f \simeq I_f^*$. For these to be *concurrently* small, the following condition
 590 must also hold

$$\frac{\pi - \Delta\beta_f}{\pi - \Delta\gamma_f} = \frac{\Delta g_f}{\Delta s_f} \quad (13)$$

591 where $\Delta\beta_f = \beta_f - \beta_f^*$, $\Delta\gamma_f = \gamma_f - \gamma_f^*$, $\Delta g_f = g_f - g_f^*$ and $\Delta s_f = s_f - s_f^*$.
 592 All these criteria, except the last one, can be tested for by making use of
 593 proper elements. The last criterion involves the proper phases which are not

594 included in the database but can, in principle, be recovered through harmonic
 595 analysis of the orbital element time series.

596 As an example, we specify an upper limit in Δe_f and $\Delta \sin I_f$ of 0.01 and
 597 a limit in Δg_f and Δs_f of 1 arcsec per year. For Ceres co-orbitals, these
 598 correspond to a maximum epicycle excursion of ~ 0.05 AU and a period
 599 of > 1 Myr in the evolution of e_r and I_r . 15 and 7 of the 39 QS librators
 600 identified in this work satisfy either of these criteria respectively but none
 601 do both. On the other hand, 2 coorbitals of Vesta do satisfy both criteria (3
 602 and 8 respectively satisfy either one). Although neither of these two objects
 603 (78994 and 139168) satisfies the condition for concurrently small e_r and I_r
 604 we find the dynamical evolution of 139168 particularly interesting and we
 605 discuss it in some detail below.

606 This asteroid has $\Delta e_f = -0.0029379$, $\Delta \sin I_f = -0.0006901$, $\Delta g_f =$
 607 0.020303 arcsec/yr and $\Delta s_f = 0.075063$ arcsec/yr. Inspection of our simu-
 608 lations of the nominal orbit of the asteroid shows that currently $e_r \sim 0.013$,
 609 $\sin I_r \sim 0.15$. Both elements are slowly increasing in time from the present
 610 with a period significantly longer than the 2×10^6 yr spanned by our inte-
 611 grations. Towards the past, The relative inclination continues to decrease
 612 with $\sin I_r \sim 0.10$ at $t = -10^6$ yr while e_r reaches a minimum of < 0.008
 613 at $t = -8.5 \times 10^5$ yr. For most of the integrated timespan, the object is a
 614 horseshoe with a very small opening angle, suggesting that it is sufficiently
 615 energetic to enter a QS mode (top left panel of Fig. 9) with $3C/8\mu \sim 3.5$.
 616 Indeed, we find two instances, indicated by the vertical arrows in the top
 617 panel of Fig. 18, when the asteroid is trapped into a QS mode for 10^4 yr
 618 and an λ_r amplitude of $\sim 1^\circ$ ($\sim 10^{-2}$ rad). Since this is comparable to e_r
 619 (middle panel), these are not, strictly speaking, RS orbits. Nevertheless, it
 620 implies that the planar component of the motion occurs within a few times
 621 $\lambda_r a$ of Vesta. In Fig. 19 we show the asteroid's motion for the phase of QS
 622 libration at $t = -3.15 \times 10^5$ yr in a heliocentric cartesian frame co-rotating
 623 with Vesta's mean motion. In the XY plane (bottom panel), the distance
 624 from Vesta varies between 10^{-2} and 8×10^{-2} AU. However, the excursion
 625 in Z (bottom panel) is significantly larger, ~ 0.3 AU. Note that the centre
 626 of the planar motion is offset from Vesta's position. This is partly because
 627 one is looking at the superposition of two harmonic modes (guiding centre
 628 and epicycle) of comparable amplitude. In addition, the potential minimum
 629 may not be exactly at $\lambda_r = 0$ since the maxima that bracket it are generally
 630 not equal unless $\omega_r = k\pi$. This becomes apparent if one expands the Hill
 631 potential to order higher than 2 or utilises the full potential of the averaged

632 motion i.e. Eq. 1.

633 Since $e_r < I_r$ the QS-enabling potential minimum at the origin exists only
 634 for values of ω_r sufficiently far from $k\pi$ while the maxima on either side are
 635 highest for $\omega_r = k\pi + \pi/2$, becoming singularities if $I_r = 0$. These are the
 636 $K > 2$ orbits of N99. We can verify that this is the case here by overplotting
 637 ω_r on the top panel of Fig. 18 (dashed curve). We find that, during QS
 638 libration, the value of ω_r is near $\pm 90^\circ$ (horizontal dotted lines) as expected.

639 Eventually, e_r and I_r will pass through their minima sufficiently closely
 640 in time to make long-term capture in a low amplitude QS mode possible.
 641 For the given values of Δg_f and Δs_f this should occur every $\sim 6.4 \times 10^7$
 642 yr. A crude estimate on the expected number of such objects may be made
 643 under the assumptions that (a) this is the only object of its type, (b) the
 644 proper element catalog is complete for MBAs with $a < 2.8$ AU down to an
 645 absolute magnitude $H \simeq 16$ and (c) the duration of QS capture is $\geq 10^5$
 646 yr, similar to large amplitude QS phases observed for other asteroids. The
 647 resulting average frequency of such objects at any one time is $\sim 1.5 \times 10^{-3}$.
 648 Adopting an absolute magnitude distribution law of $10^{0.3H}$ (Gladman et al.,
 649 2009), we find that the frequency reaches unity for $H \sim 26$ or $D = 12 - 37$
 650 m objects. Unlike large amplitude Quasi-Satellites, the cartesian velocity of
 651 such objects with respect to Vesta is not high. For 139168 it ranges from
 652 2.2 to 3.2 km sec $^{-1}$ for the integration spanning the last 1 Myr and will
 653 be lower if I_r is smaller. Hence, and in view of possible *in situ* satellite
 654 searches by missions such as DAWN (Cellino et al., 2006), newly discovered
 655 objects in apparent proximity to Vesta in the sky would need to be carefully
 656 followed up to determine whether they are “true” (ie keplerian) satellites or
 657 small-amplitude Quasi-Satellites.

658 7. Conclusions and Discussion

659 In this work we have demonstrated the existence of a population of Main
 660 Belt Asteroids (MBAs) in the coorbital resonance with the large asteroid
 661 (4) Vesta and the dwarf planet (1) Ceres. Libration within the resonance
 662 is transient in nature; our integrations show that these episodes can last for
 663 $> 2 \times 10^6$ yr. Partly due to the significant eccentricities and inclinations of
 664 these asteroids, we find that their dynamics are similar to those that govern
 665 the evolution of near-Earth asteroids in the 1:1 resonance with the Earth and
 666 Venus. However, due to the high density of objects as a function of semi-
 667 major axis, a steady state population of ~ 50 co-orbitals of Ceres and ~ 45

668 of Vesta is maintained. Apart from the natural dynamics of eccentric and
 669 inclined 1:1 librators, we identify two other mechanisms which contribute to
 670 the temporary nature of these objects. One is the inherent chaoticity of the
 671 orbits; with some exceptions, particles started in neighbouring orbits evolve
 672 apart over 10^5 yr timescales. The other is close encounters with massive
 673 asteroids that do not participate in the Sun-Secondary-Particle three body
 674 problem. We show individual cases of asteroids leaving the coorbital reso-
 675 nance with Vesta following a deep encounter with Ceres. It is not clear if
 676 the latter effect is significant at the population level. It may be adversely
 677 affecting the occurrence of long-lived tadpole librators of Vesta. Finally, we
 678 show that bound or Quasi-Satellite orbits around both Ceres and Vesta can
 679 exist and identify 3 current Quasi-Satellite librators around Ceres as well as
 680 an object which may experience episodes of long-lived bound motion within
 681 a few times 10^{-2} AU from Vesta.

682 The demonstration of a resonant mechanism within the asteroid belt
 683 which acts independently of the major planets raises some interesting ques-
 684 tions to be addressed by future work. One of these is whether there exists a
 685 threshold below which a mass becomes a particle in real planetary systems.
 686 In partial response to this question - and as part of the integrations reported
 687 in Section 3 - we simulated the motion of several MBAs with proper semi-
 688 major axes within the coorbital region of 2 Pallas and 10 Hygiea. None of
 689 these was trapped in co-orbital libration which leads us to conclude that this
 690 threshold for the solar system's Main Asteroid Belt is $\sim 10^{-10}$ solar masses.
 691 However, this may not be true of other planetary systems with fewer and/or
 692 less massive planets. We speculate that co-orbital trapping of planetesimals
 693 by terrestrial planets or large asteroids may give rise to observationally verifi-
 694 able dynamical structures. This is not a new idea (eg Moldovan et al., 2010)
 695 but our results show that even small bodies ($10^{-10} < \mu < 10^{-6}$) can maintain
 696 transient populations of Trojans in a steady state and that the dynamical
 697 excitation of planetesimals in a disk does not necessarily imply that the coor-
 698 bital resonance becomes ineffective. In this context, it may be relevant to the
 699 dynamical evolution of the larger planetesimals in protoplanetary disks and
 700 the planets or protoplanet cores embedded within them (Papaloizou et al.,
 701 2007).

702 **Acknowledgements**

703 The authors would like to thank Dr Fathi Namouni for kindly answering
704 our numerous questions regarding eccentric and inclined coorbital motion.
705 Part of this work was carried out during a visit of AAC at UWO, funded
706 by NASA’s Meteoroid Environment Office (MEO). Astronomical research at
707 the Armagh Observatory is funded by the Northern Ireland Department of
708 Culture, Arts and Leisure (DCAL).

709 **References**

- 710 Brasser, R., Huang, T.-Y., Mikkola, S., Wiegert, P., Innanen, K. A., 2004.
 711 Long-term evolution of the Neptune Trojan 2001 QR322. *Mon. Not. R. As-*
 712 *tron. Soc.* 347, 833–836.
- 713 Cellino, A., Capaccioni, F., Capria, M. T., de Sanctis, M. C., Keller, H. U.,
 714 Prettyman, T. H., Raymond, C. A., Russell, C. T., 2006. Understanding
 715 the origin of the asteroids through the study of Vesta and Ceres: The role
 716 of DAWN. *Adv. Geophys.* 3, 287–298.
- 717 Chambers, J. E., 1999. A hybrid symplectic integrator that permits close
 718 encounters between massive bodies. *Mon. Not. R. Astron. Soc.* 304, 793–
 719 799.
- 720 Christou, A. A., 2000a. A numerical survey of transient co-orbitals of the
 721 terrestrial planets. *Icarus* 144, 1–20.
- 722 Christou, A. A., 2000b. Co-orbital objects in the main asteroid belt. *As-*
 723 *tron. Astrophys.* 356, L71–L74.
- 724 Everhart, E., 1985. An efficient integrator that uses Gauss-Radau spacings.
 725 In: Carusi A., Valsecchi, J. (Eds.) *Dynamics of Comets: Their Origin and*
 726 *Evolution*, Reidel, Dordrecht, 185–202.
- 727 Giorgini, J. D., Yeomans, D. K., Chamberlin, A. B., Chodas, P. W., Jacob-
 728 son, R. A., Keesey, M. S., Lieske, J. H., Ostro, S. J., Standish E. M., Wim-
 729 berly, R. N., 1996. JPL’s on-line Solar System data service. *Bull. Am. As-*
 730 *tron. Soc.* 28, 1158.
- 731 Gladman, B., Davis, D., Neese, C., Jedicke, R., Williams, G., Kavelaars,
 732 J., Petit, J.-M., Holman, M., Harrington, B., Esquerdo, G., Tricarico, P.,
 733 2009. On the asteroid belt’s orbital and size distribution. *Icarus* 202, 104–
 734 118.
- 735 Hénon, M., 1969. Numerical exploration of the restricted problem. V. Hill’s
 736 case: Periodic orbits and their stability. *Astron. Astrophys.* 1, 223–228.
- 737 Hénon, M., Guyot, M., 1970. Stability of periodic orbits in the re-
 738 stricted three-body problem. In: *Periodic Orbits, Stability and Resonances*
 739 (G. E. O. Giacaglia, Ed.), Reidel, Dordrecht, 349–374.

- 740 Jackson, J., 1913. Retrograde satellite orbits. *Mon. Not. R. Astron. Soc.* 74,
741 62–82.
- 742 Knežević, Z., Milani, A., 2000. Synthetic proper elements for outer main belt
743 asteroids. *Cel. Mech. Dynam. Astron.* 78, 17–46.
- 744 Konopliv, A. S., Yoder, C. F., Standish, E. M., Yuan, D.-N., Sjogren, W. L.,
745 2006. A global solution for the Mars static and seasonal gravity, Mars
746 orientation, Phobos and Deimos masses, and Mars ephemeris. *Icarus* 182,
747 23–50.
- 748 Levison, H., Shoemaker, E. M., Shoemaker, C. S., 1997. The dispersion of
749 the trojan asteroid swarm. *Nature* 385, 42–44.
- 750 Lissauer, J., Goldreich, P., Tremaine, S., 1985. Evolution of the Janus-
751 Epimetheus coorbital resonance due to torques from Saturn’s rings. *Icarus*
752 64, 425–434.
- 753 Message, P. J., 1966. *Lectures in Applied Mathematics* 6, 70.
- 754 Mikkola, S., Brasser, R., Wiegert, P., Innanen, K., 2004. Asteroid 2002 VE68,
755 a quasi-satellite of Venus. *Mon. Not. R. Astron. Soc.* 351, L63–L65.
- 756 Mikkola, S., Innanen, K., 1997. Orbital stability of planetary quasi-satellites.
757 In: Dvorak, R., Henrard, J. (Eds), *The Dynamical Behaviour of our Plan-*
758 *etary System, Proceedings of the Fourth Alexander von Humboldt Collo-*
759 *quium on Celestial Mechanics*, Kluwer Academic Publishers, 345.
- 760 Milani, A., Knežević, Z., 1994. Asteroid proper elements and the dynamical
761 structure of the asteroid main belt. *Icarus* 107, 219–254.
- 762 Moldovan, R., Matthews, J. M., Gladman, B., Bottke, W. F., Vokrouhlický,
763 D., 2010. Searching for Trojan Asteroids in the HD 209458 System: Space-
764 based MOST Photometry and Dynamical Modeling. *Astrophys. J.* 716,
765 315–323.
- 766 Morais, M. H. M., 1999. A secular theory for Trojan-type motion. *Astron. As-*
767 *trophys.* 350, 318–326.
- 768 Morais, M. H. M., 2001. Hamiltonian formulation of the secular theory for
769 Trojan-type motion. *Astron. Astrophys.* 369, 677–689.

770 Morais, M. H. M., Morbidelli, A., 2002. The population of NEAs in coorbital
771 motion with the Earth. *Icarus* 160, 1–9.

772 Morais, M. H. M., Morbidelli, A., 2006. The population of NEAs in coorbital
773 motion with Venus. *Icarus* 185, 29–38.

774 Murray, C. D., Cooper, N. J., Evans, M. W., Beurle, K., 2005. S/2004 S 5:
775 A new co-orbital companion of Dione. *Icarus* 179, 222–234.

776 Murray, C. D., Dermott, S. F., 1999. *Solar System Dynamics*. Cambridge
777 University Press, Cambridge.

778 Namouni, F., 1999. Secular interactions of coorbiting objects. *Icarus* 137,
779 293–314.

780 Namouni, F., Christou, A. A., Murray, C. D., 1999. Coorbital dynamics at
781 large eccentricity and inclination. *Phys. Rev. Lett.* 83, 2506–2509.

782 Nesvorný, D., Roig, F., Ferraz-Mello, S., 2000. Close approaches of trans-
783 Neptunian objects to Pluto have left observable signatures on their orbital
784 distribution. *Astron. J.* 119, 953–969.

785 Papaloizou, J. C. B., Nelson, R. P., Kley, W., Masset, F., Artymowicz, P.,
786 2007. Disk-planet interactions during planet formation. In: Reipurth, B.,
787 Jewitt, D. and Keil, K. (Eds), *Protostars and Planets V*, University of
788 Arizona Press, Tucson, 655–668.

789 Scholl, H., Marzari, F., Tricarico, P., 2005. Dynamics of Mars Trojans. *Icarus*
790 175, 397–408.

791 Sheppard, S. S., Trujillo, C. A., 2006. A thick cloud of Neptune Trojans and
792 their colors. *Science* 313, 511–514.

793 Wajer, P., 2010. Dynamical evolution of Earth’s quasi-satellites: 2004 GU9
794 and 2006 FV35. *Icarus* 209, 488–493.

795 Wiegert, P., Innanen, K., Mikkola, S., 1997. An asteroidal companion to the
796 Earth. *Nature* 387, 685–686.

797 Wiegert, P. A., Innanen, K. A., Mikkola, S., 1998. The orbital evolution of
798 near-Earth asteroid 3753. *Astron. J.* 115, 2604–2613.

- 799 Wiegert, P. A., Innanen, S., Mikkola, S., 2000. The stability of quasi-satellites
800 in the outer solar system. *Astron. J.* 119, 1978–1978.
- 801 Wisdom, J., Holman, M., 1992. Symplectic maps for the n-body problem -
802 Stability analysis. *Astron. J.* 104, 2022–2029.
- 803 Yu, Q. J., Tremaine, S., 1999. The dynamics of Plutinos. *Astron. J.* 118,
804 1873–1881.

805 List of Figures

806	1	Comparison of proper, averaged and osculating semimajor axis	
807		for asteroid 1372 Haremary during a numerical 10^4 yr numerical	
808		integration of its orbit. See text for details.	34
809	2	Examples of dynamical evolution of specific asteroids coorbit-	
810		ing with Ceres as determined by our numerical integrations	
811		over 2×10^6 yr. The upper row shows the evolution of the	
812		relative semimajor axis a_r while the bottom row that of the	
813		relative longitude λ_r	35
814	3	As Fig. 2 but for coorbitals of Vesta.	36
815	4	Dynamical evolution of 600 clones of asteroids 65313 (Ceres	
816		coorbital; top left), 76146 (Ceres coorbital; top right), 81522	
817		(Ceres coorbital; centre left), 129109 (Ceres coorbital; centre	
818		right), 156810 (Vesta coorbital; bottom left) and 185105	
819		(Ceres coorbital; bottom right) for 10^6 yr as explained in the	
820		text.	37
821	5	Histograms of the statistical distribution of co-orbital aster-	
822		oids of Ceres (upper panel) and Vesta (lower panel) within	
823		the coorbital regions of these massive asteroids as quantified	
824		by the relative proper semimajor axis $a_{r, p}$	38
825	6	Histograms of the statistical distribution of different types of	
826		Ceres (top) and Vesta (bottom) co-orbital asteroids divided	
827		over the total number of asteroids in each bin. The x-axis is	
828		in the same units as Fig. 5.	39
829	7	Proper element distribution of different types of Ceres (top)	
830		and Vesta (bottom) co-orbital asteroids. The two left pan-	
831		els show the proper eccentricity as a function of the relative	
832		proper semimajor axis (units of ϵ as in Fig. 5) while the right	
833		two panels show the proper inclination.	40
834	8	Histogram of the relative longitudes λ_r of asteroids currently	
835		coorbiting with Ceres (upper panel) or Vesta (lower panel).	
836		The position of the secondary ($\lambda_r = 0$) is at bin 6. Counts	
837		have been normalised to the average value per bin.	41

838	9	Model fits to the motion of Ceres (top row) and Vesta (bottom	
839		row) coorbital MBAs shown in Figs 2 and 3 respectively. The	
840		curve, horizontal line and dotted circle correspond to the profile	
841		of S (Eq. 2), the quantity $3C/8\mu$ and the point $(\lambda_r, 3C/8\mu)$	
842		respectively at $t = 0$ as functions of the relative longitude λ_r	
843		in degrees.	42
844	10	Dynamical evolution of 300 clones of asteroids 129109, 156810	
845		and 185105 (left, centre and middle column respectively) for	
846		the three models discussed in the text.	43
847	11	Histograms of numbers of encounters ($< 5R_H$) of Ceres co-	
848		orbitals with massive asteroids in our three models. Bins have	
849		been normalised by the total number of objects in each per-	
850		sistency class.	44
851	12	As Fig. 11 but for Vesta co-orbitals.	45
852	13	Histograms of numbers of encounters of Ceres co-orbitals with	
853		massive asteroids as a function of encounter distance in the	
854		three models described in Section 5.	46
855	14	As Fig. 13 but for Vesta co-orbitals.	47
856	15	Two examples of coorbitals of Vesta ejected from the resonance	
857		after close encounters with Ceres. The vertical arrows indicate	
858		the moment of encounter with Ceres ('C') while the number	
859		in brackets is the closest approach distance in R_H	48
860	16	Two examples of MBAs that exhibited Quasi-Satellite libra-	
861		tion with Ceres and Vesta in our simulations. The position of	
862		the Sun is indicated by the character 'S'.	49
863	17	Histogram of the relative proper semimajor axis (in units of ϵ)	
864		of those MBAs that persisted in coorbital libration (blue line)	
865		and those that became temporary quasi-satellites (red line) of	
866		Ceres (left) and Vesta (right).	50
867	18	Detail of the past dynamical evolution of 139168 in our simu-	
868		lations. The arrows indicate instances when the asteroid be-	
869		came an eccentric retrograde satellite of Vesta with λ_r almost	
870		stationary at 0°	51

871	19	Motion of 139168 with respect to Vesta in cartesian ecliptic	
872		coordinates during an episode of QS capture at $t \simeq -3 \times 10^5$	
873		yr indicated in Fig. 18. The dashed lines mark the location	
874		$x = a_{p, \text{ Vesta}} \simeq 2.3615$ au, $y = z = 0$. Note the large amplitude	
875		of the vertical motion (right panel) compared to the planar	
876		projection (left panel).	52

Table 1: Dynamical parameters of large asteroids considered in this work. See text for details.

	Ceres	Vesta	Pallas	Hygiea
$\mu \times 10^{10}$	4.699	1.358	1.026	0.454
$\epsilon \times 10^4$	5.42	3.56	3.25	2.47
a_{proper} (AU)	2.7670962	2.3615126	2.7709176	3.1417827
$\epsilon a_{\text{proper}} (\times 10^4 \text{AU})$	15.0	8.4	9.0	7.8

Table 2: Statistical results of the numerical simulations reported in Section 3. See text for details.

	Full	Now	L ₄ Tadpole	L ₅ Tadpole
Ceres	129	51	15 (2)	4 (2)
Vesta	94	44	5	7 (1)
	Horseshoe	Transition	QS	Always
Ceres	20	11	1	18
Vesta	21	11	0	10

Table 3: Estimated mean and Full Width at Half Maximum (FWHM) of distributions presented in Fig. 6.

	All coorbitals		Current coorbitals		Persistent coorbitals	
	μ	FWHM	μ	FWHM	μ	FWHM
Ceres	$-0.029^{\pm 0.011}$	$0.341^{\pm 0.021}$	$-0.019^{\pm 0.002}$	$0.169^{\pm 0.005}$	$-0.023^{\pm 0.001}$	$0.096^{\pm 0.001}$
Vesta	$-0.006^{\pm 0.009}$	$0.301^{\pm 0.019}$	$-0.011^{\pm 0.005}$	$0.151^{\pm 0.009}$	$-0.010^{\pm 0.001}$	$0.052^{\pm 0.002}$

Table 4: Results of the numerical simulations for the models described in Section 5. See text for details.

Secondary Body	Ceres/Vesta Only		No Pallas		All Massive Asteroids	
	Persistent	Single Mode	Persistent	Single Mode	Persistent	Single Mode
Ceres	26/129	6/129	28/129	14/129	32/129	15/129
Vesta	23/94	11/94	18/94	3/94	18/94	6/94

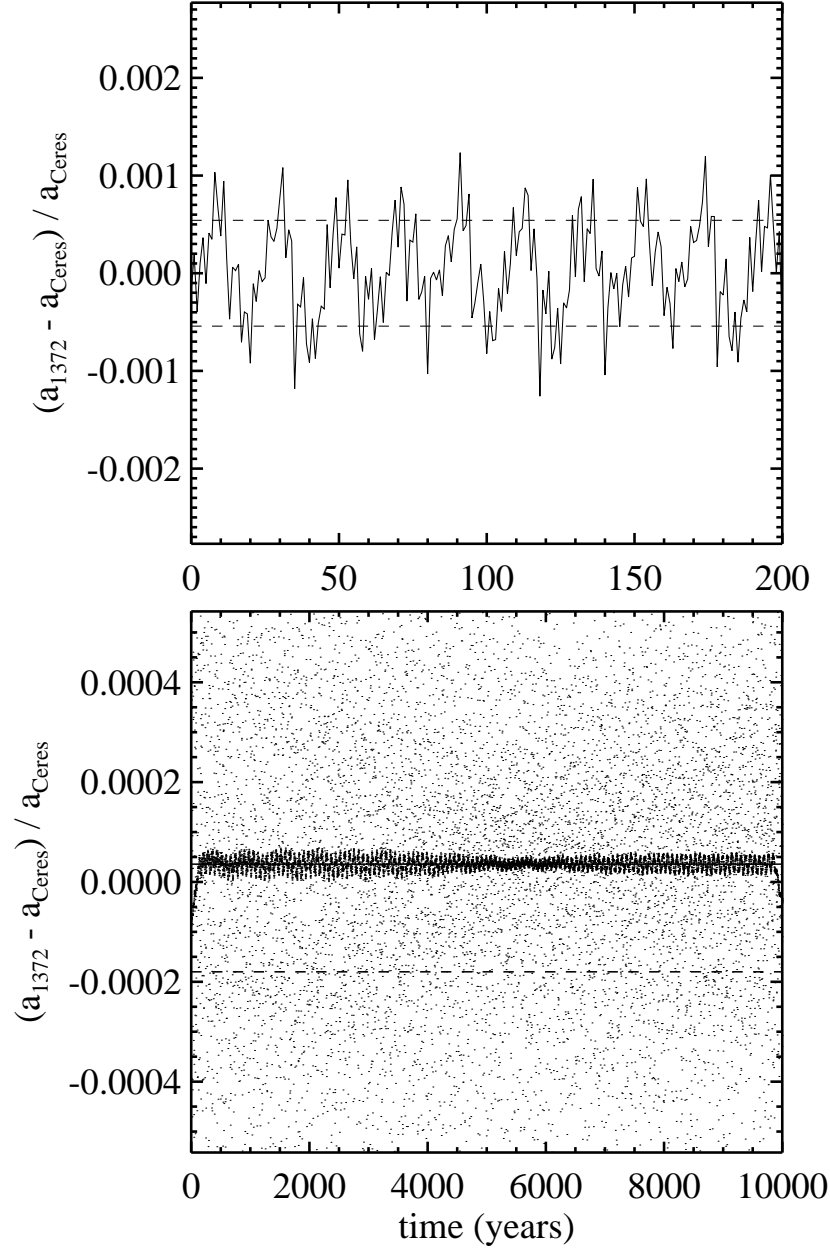


Figure 1: Christou and Wiegert 2010, Coorbitals of Ceres and Vesta

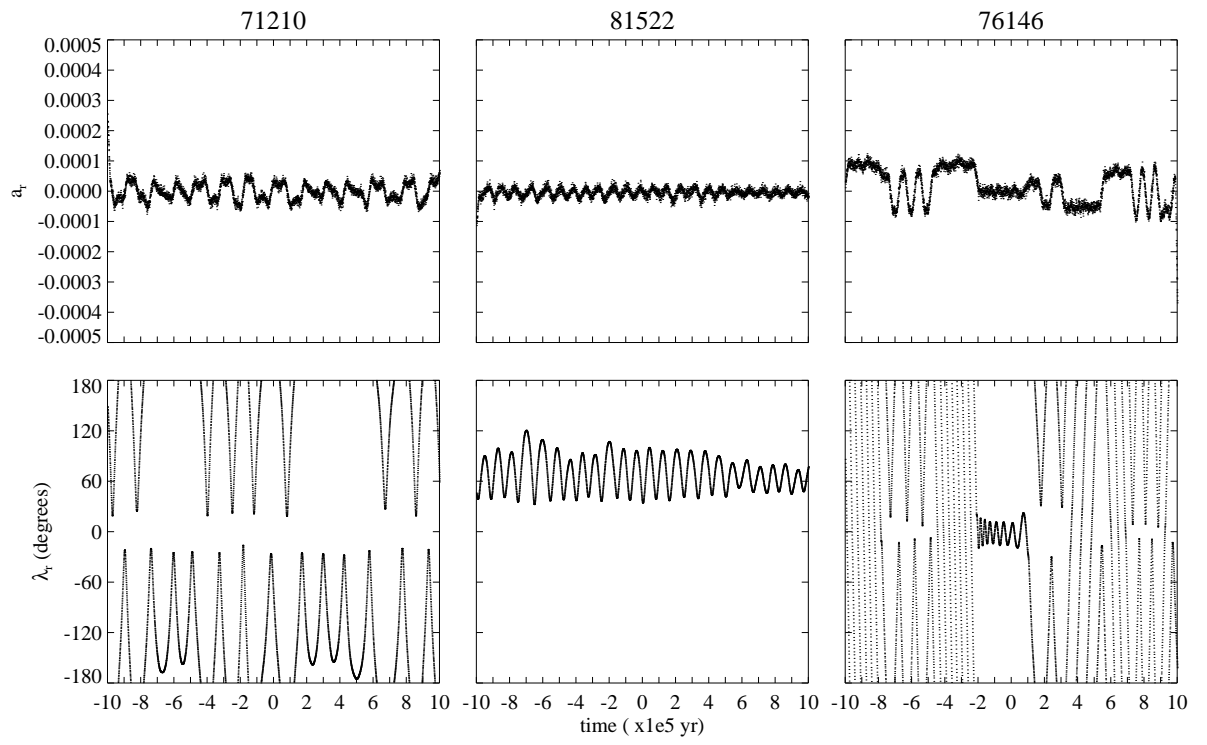


Figure 2: Christou and Wiegert 2010, Coorbitals of Ceres and Vesta

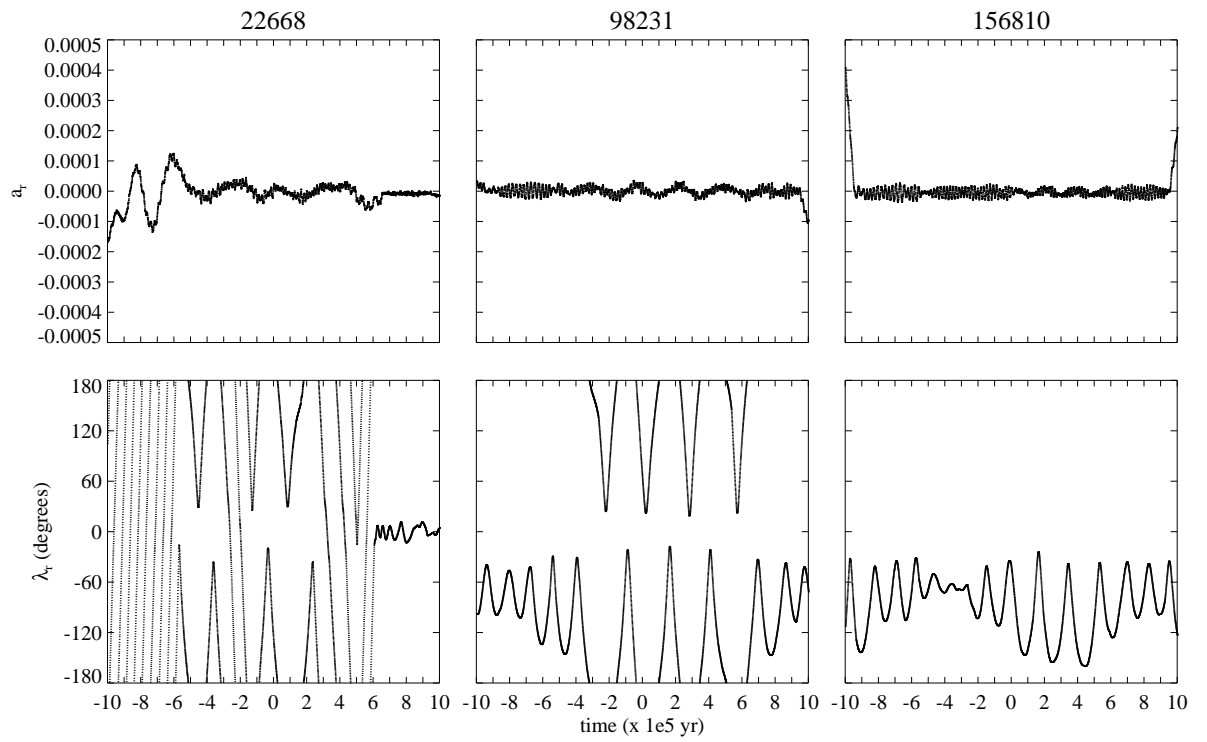


Figure 3: Christou and Wiegert 2010, Coorbitals of Ceres and Vesta

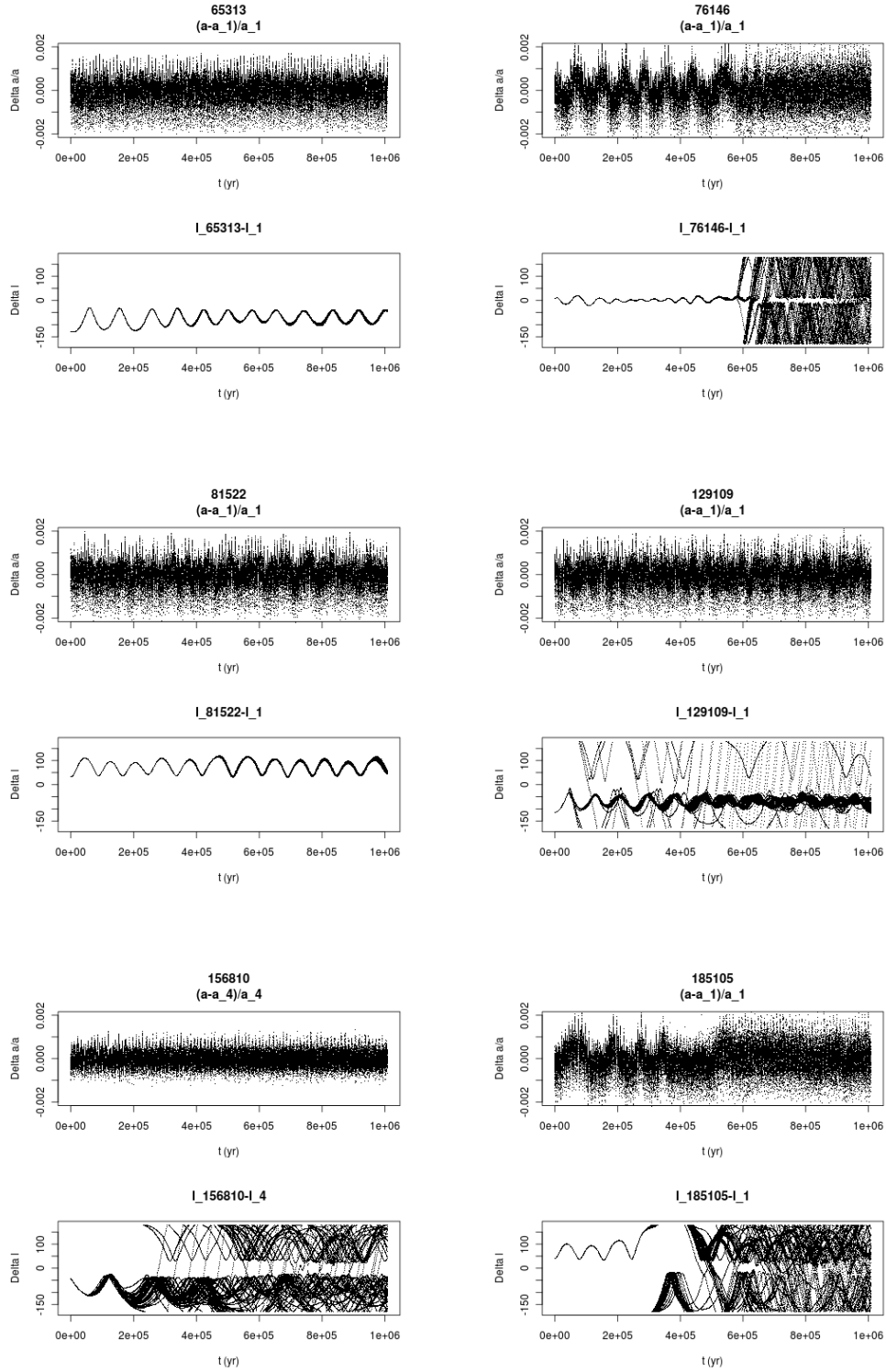


Figure 4: Christou and Wiegert 2010, Coorbitals of Ceres and Vesta

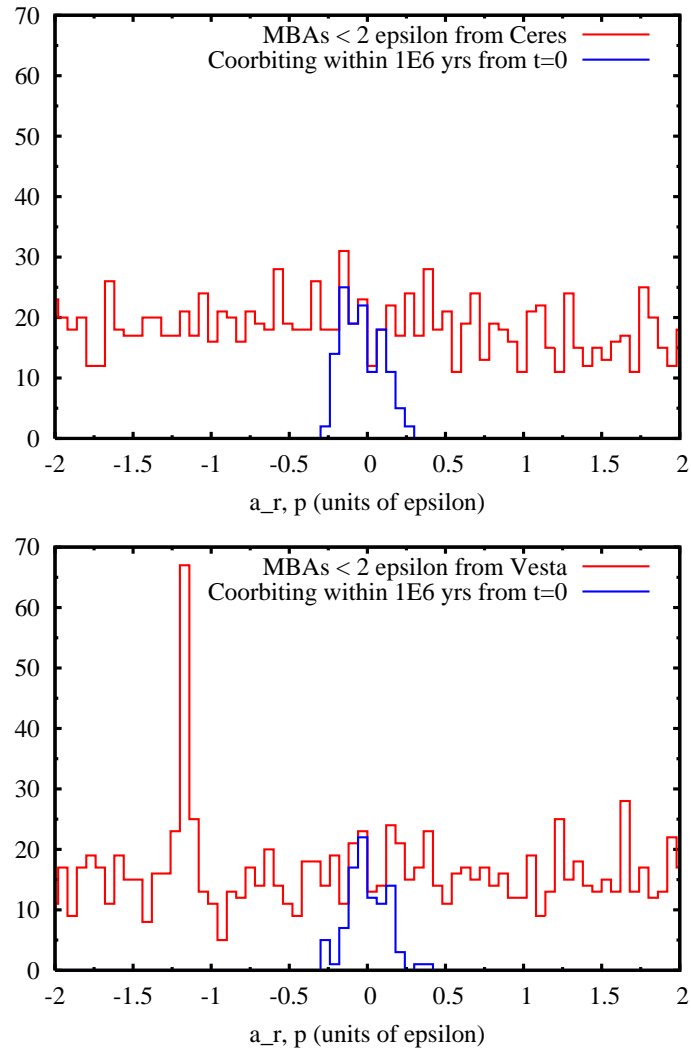


Figure 5: Christou and Wiegert 2010, Coorbitals of Ceres and Vesta

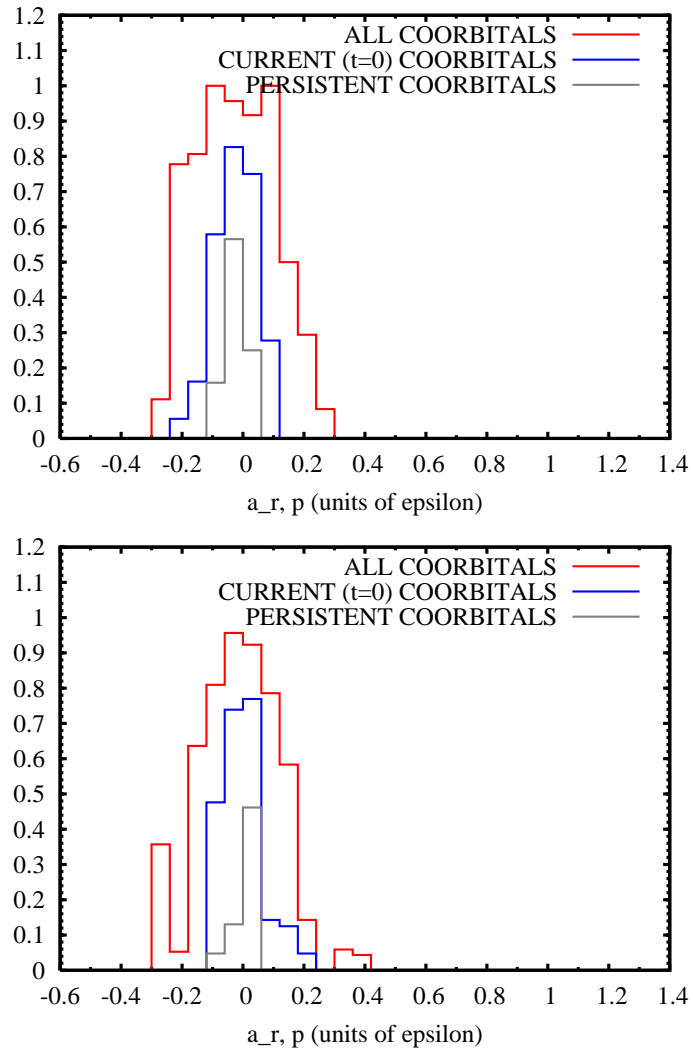


Figure 6: Christou and Wiegert 2010, Coorbitals of Ceres and Vesta

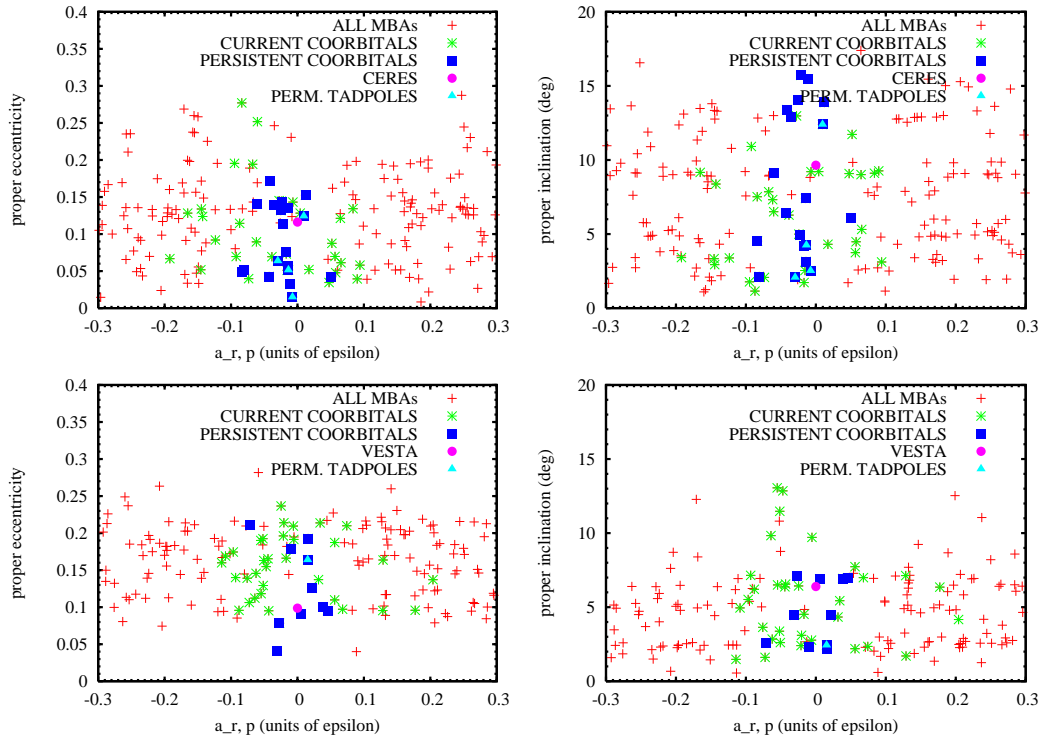


Figure 7: Christou and Wiegert 2010, Coorbitals of Ceres and Vesta

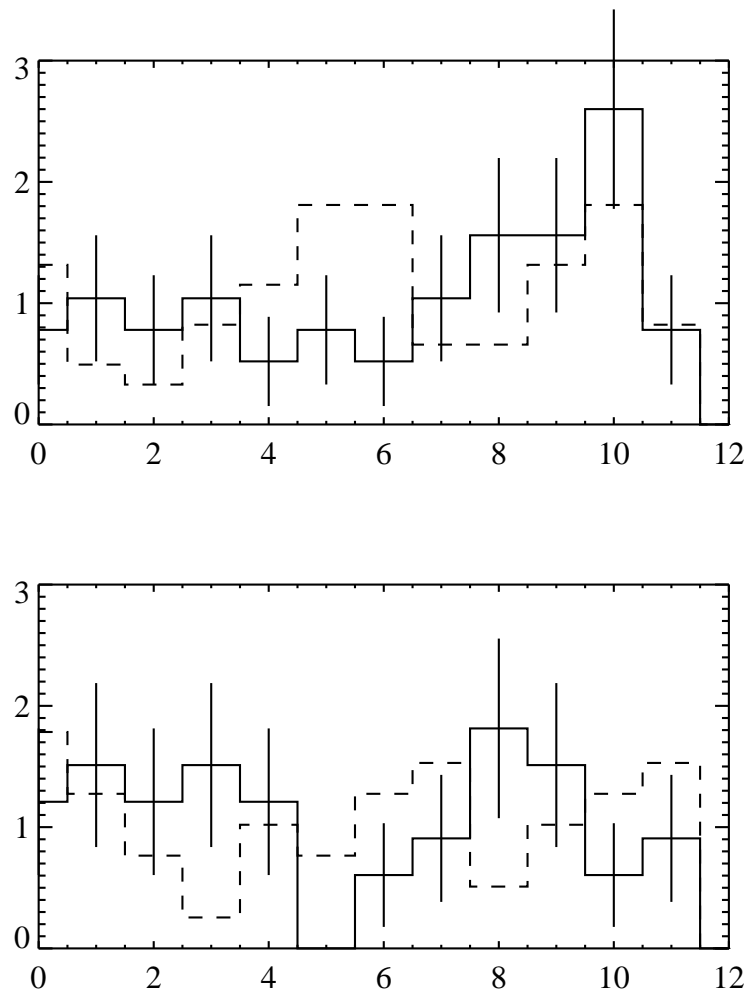


Figure 8: Christou and Wiegert 2010, Co-orbitals of Ceres and Vesta

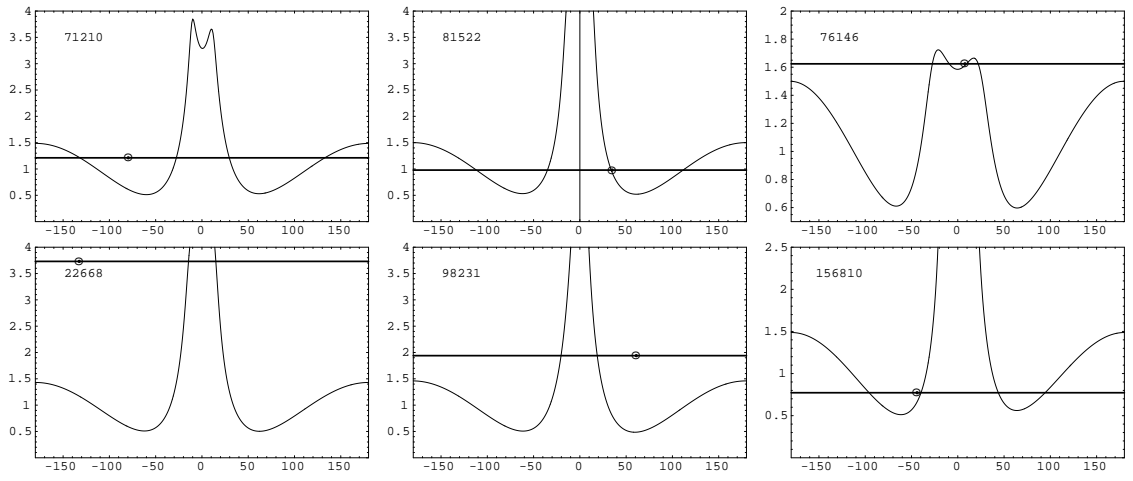


Figure 9: Christou and Wiegert 2010, Coorbitals of Ceres and Vesta

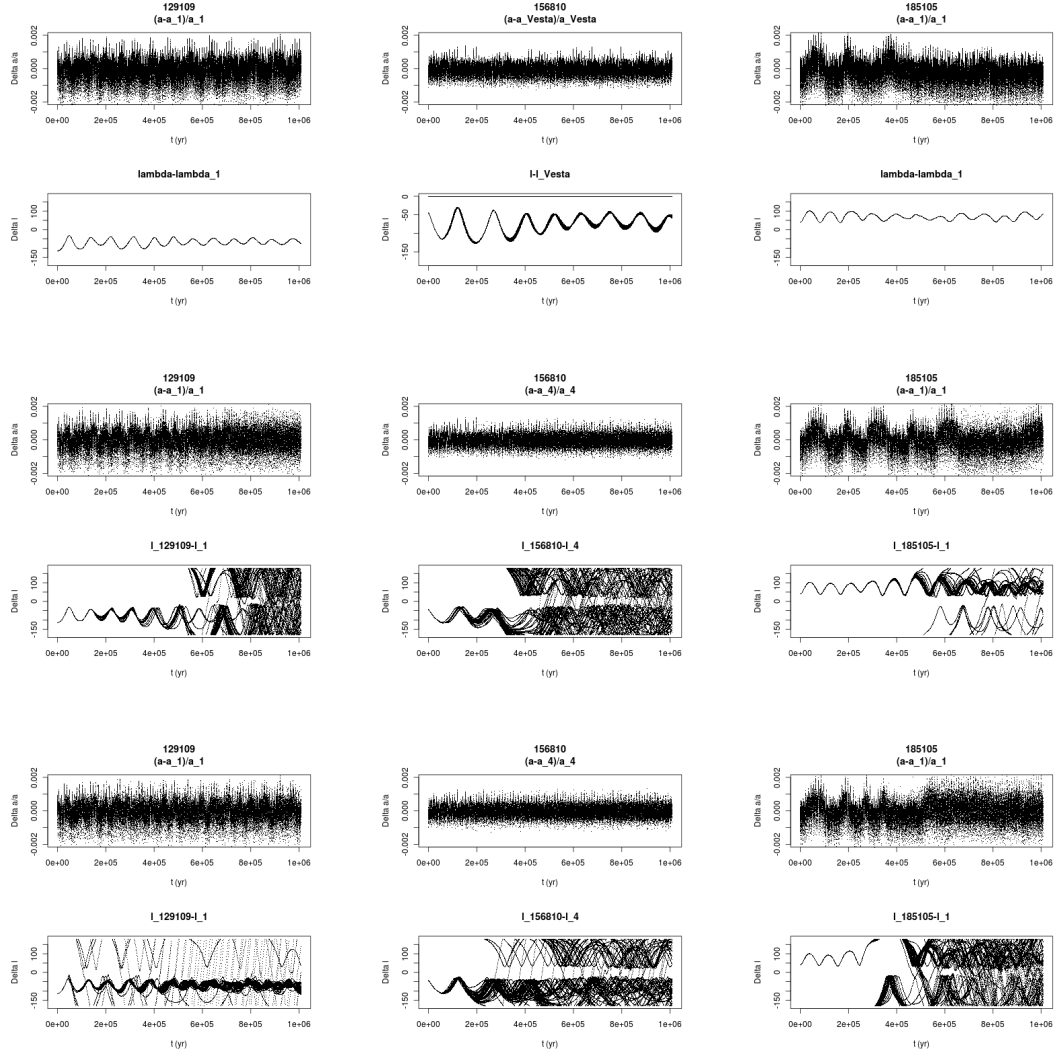


Figure 10: Christou and Wiegert 2010, Coorbitals of Ceres and Vesta

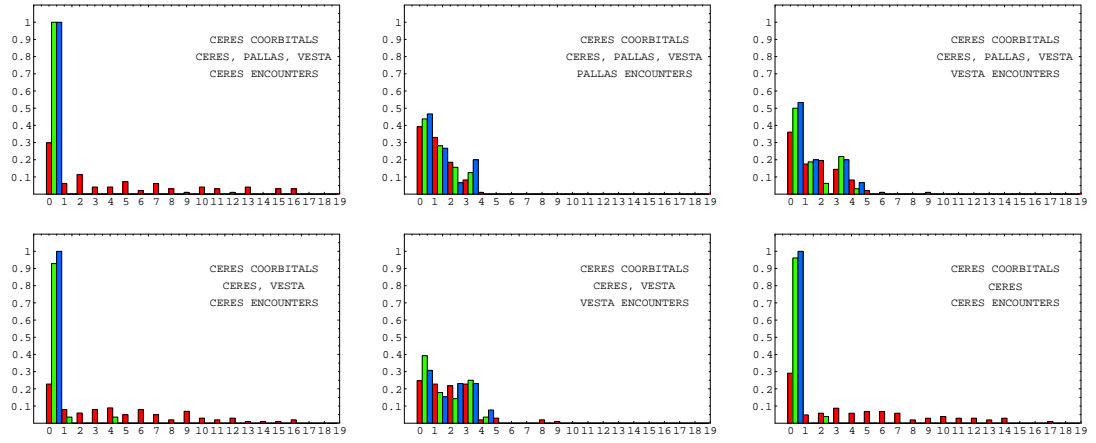


Figure 11: Christou and Wiegert 2010, Coorbitals of Ceres and Vesta

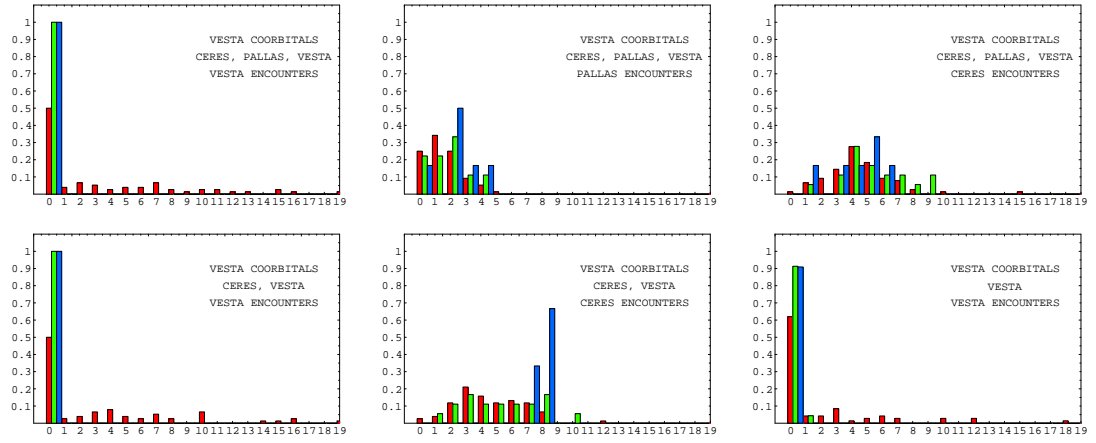


Figure 12: Christou and Wiegert 2010, Coorbitals of Ceres and Vesta

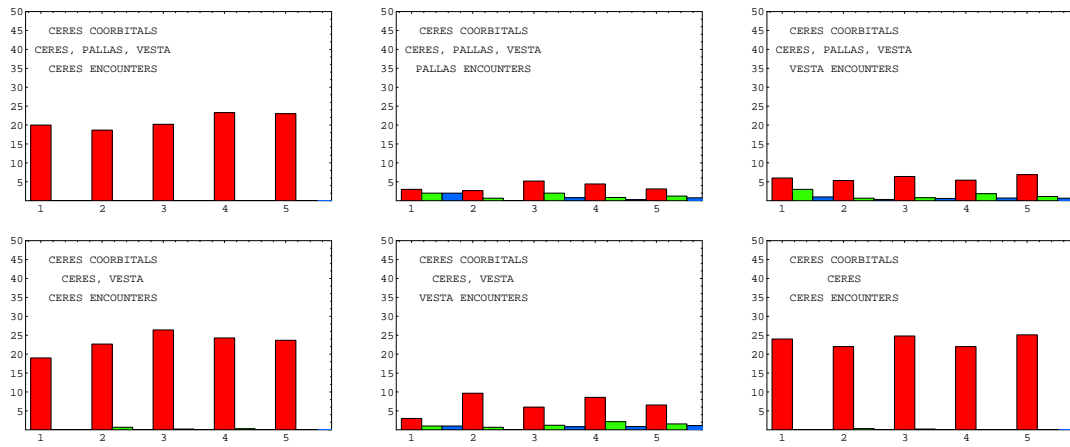


Figure 13: Christou and Wiegert 2010, Coorbitals of Ceres and Vesta

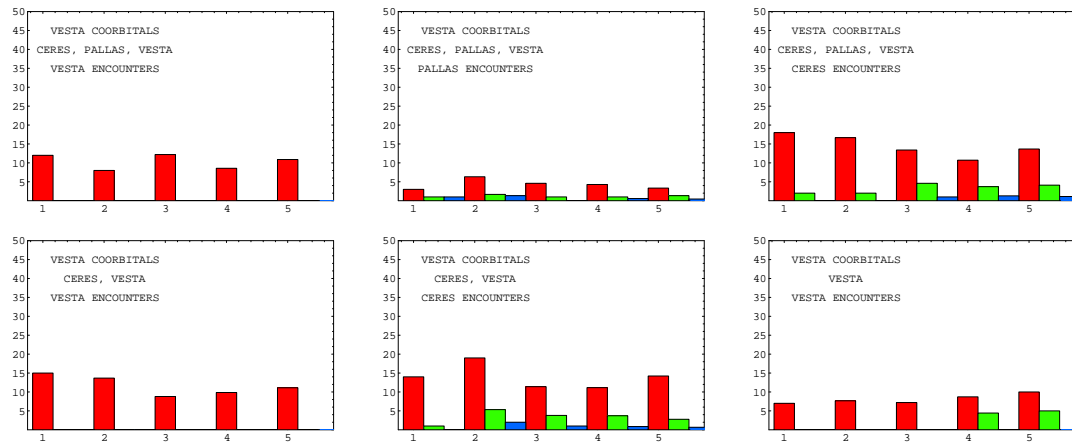


Figure 14: Christou and Wiegert 2010, Coorbitals of Ceres and Vesta

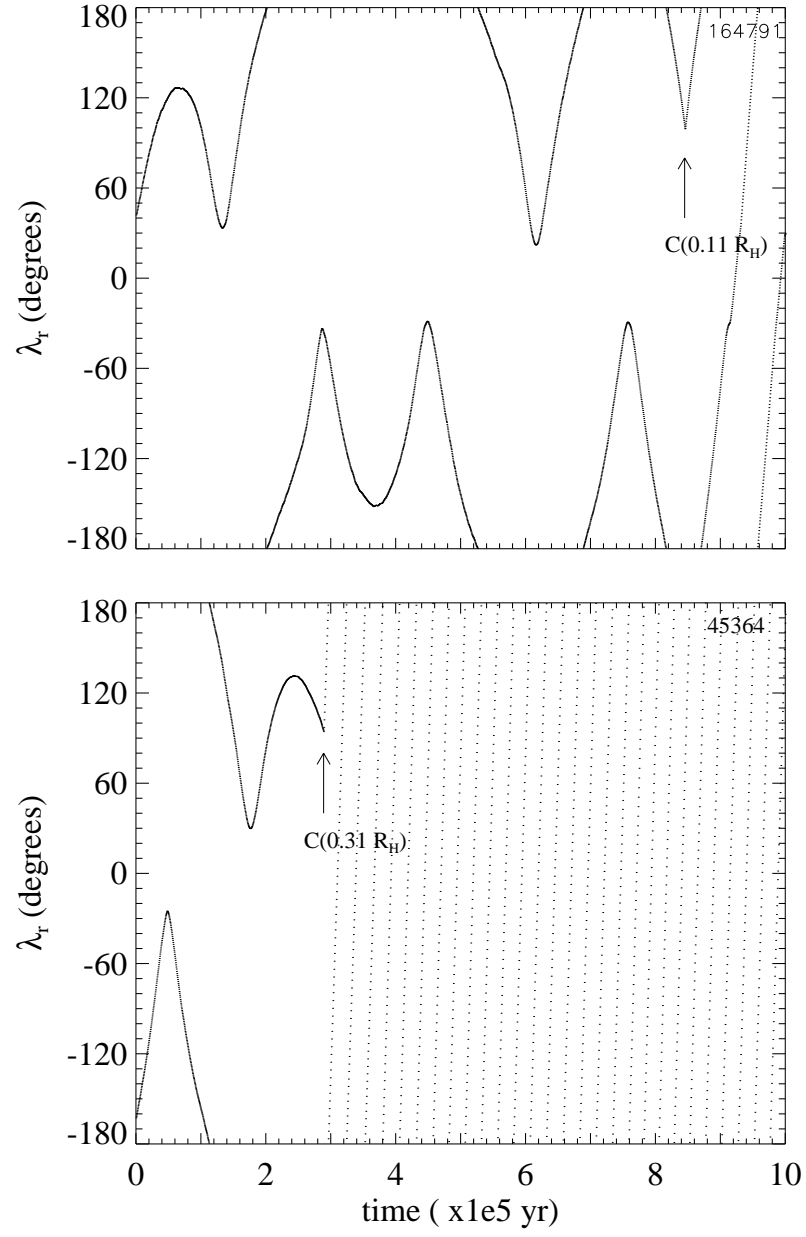


Figure 15: Christou and Wiegert 2010, Coorbitals of Ceres and Vesta

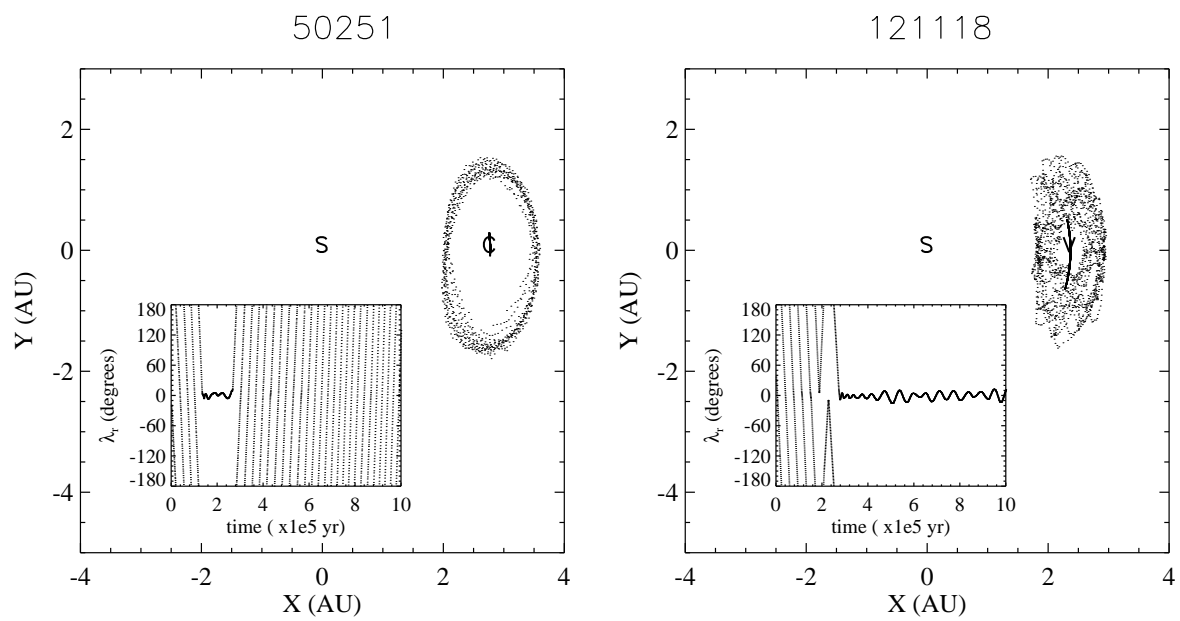


Figure 16: Christou and Wiegert 2010, Co-orbitals of Ceres and Vesta

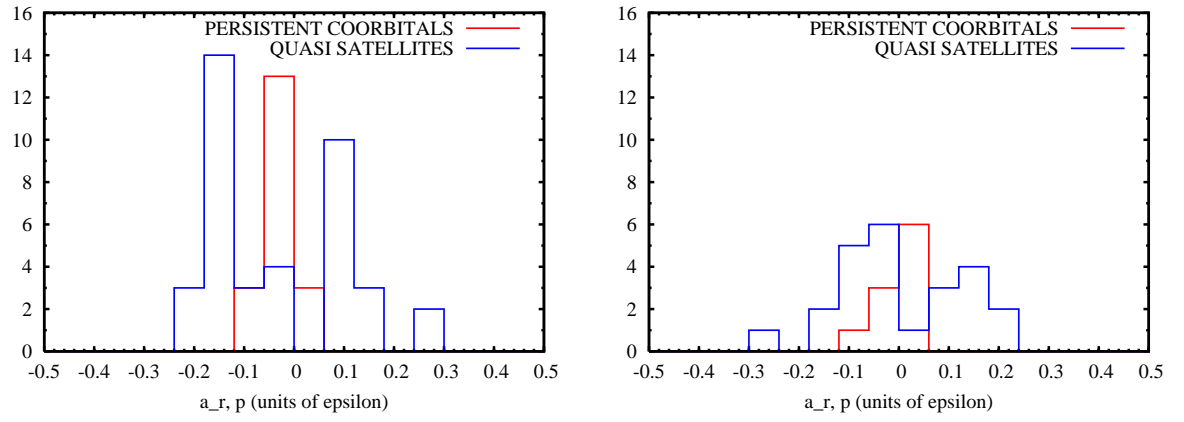


Figure 17: Christou and Wiegert 2010, Coorbitals of Ceres and Vesta

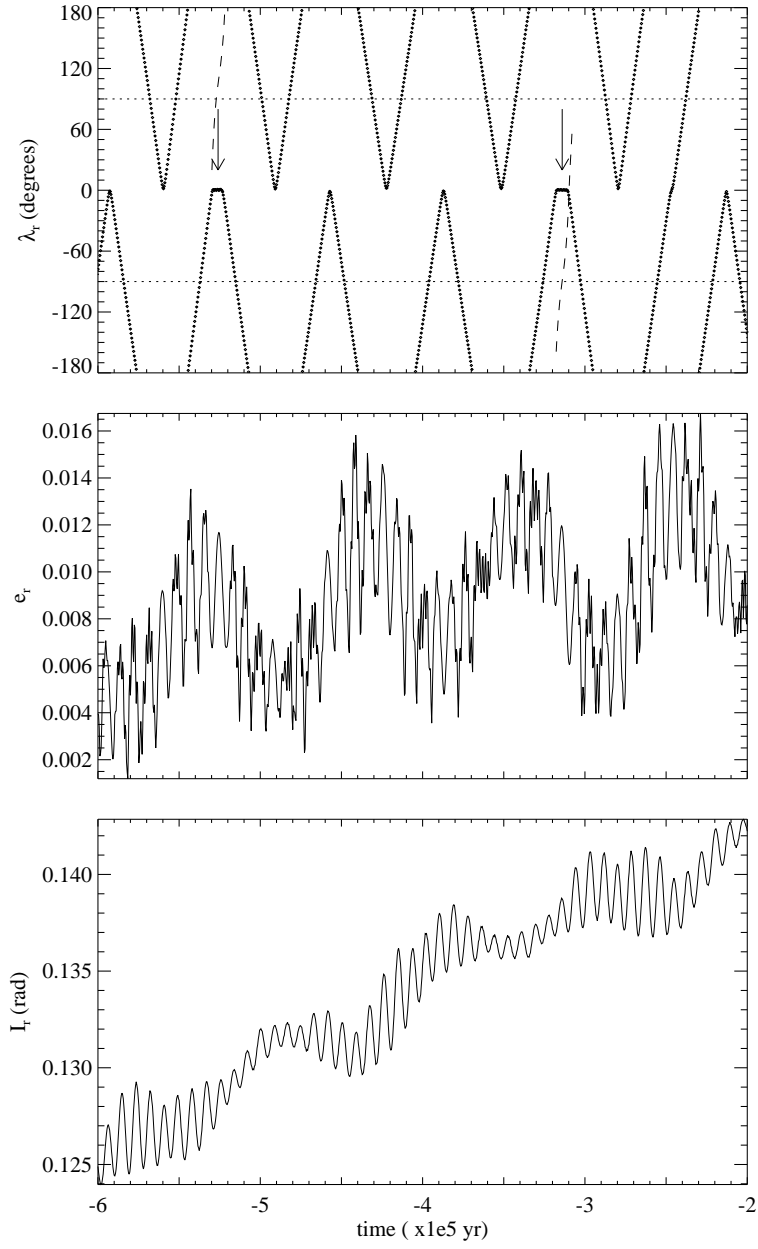


Figure 18: Christou and Wiegert 2010, Coorbitals of Ceres and Vesta

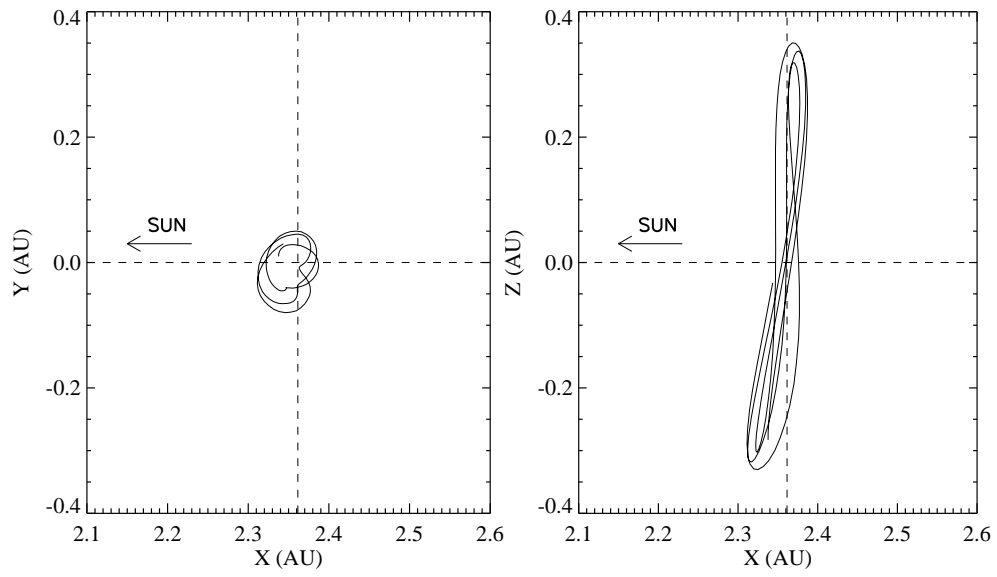


Figure 19: Christou and Wiegert 2010, Coorbitals of Ceres and Vesta